Effects of acoustic fields on the dynamics of micro-particles in a fluidized bed

Zhu, L.

Award date:
2019

TECHNISCHE UNIVERSITEIT EINDHOVEN

MASTERS THESIS

Effects of Acoustic Fields on the Dynamics of Micro-particles in a Fluidized Bed

Author:
Linhang ZHU

Supervisor:
Dr. Y TANG

A thesis submitted in fulfillment of the requirements for the degree of Master

in the

Power and Flow
Mechnical Engineering

May 14, 2019

TECHNISCHE UNIVERSITEIT EINDHOVEN

Abstract

Faculty Name
Mechnical Engineering

Master

Effects of Acoustic Fields on the Dynamics of Micro-particles in a Fluidized Bed

by Linhang ZHU

The flow behaviors of cohesive micro particles in a pseudo-2D sound-assisted fluidized bed are investigated by the mean of computational Fluid Dynamics(CFD)-Discrete Element Method(DEM) simulation. Considering van der Waals force as the cohesive force, by applying acoustic fields with different sound pressure levels and frequencies, the fluidization performance of cohesive particles in terms of pressure drop, bed expansion, particle velocity, bubble size and agglomeration size are studied. It is found that particles tend to form large agglomerates when they are strongly cohesive. The application of acoustic field induces the breakup of the formed agglomerates, while the size of agglomerates decreases with increasing sound pressure level and reaches a minimum at a useful range of sound frequency between 80Hz to 100Hz.

Contents

List of Figures

List of Tables

List of Abbreviations

FBR	**F**luidized **B**ed **R**eactor
CFD	**C**omputational **F**luid **D**ynamics
DEM	**D**iscrete **E**lement **M**ethod
SPL	**S**ound **P**ressure **L**evel
PDF	**P**robability **D**ensity **F**unction

Physical Constants

Speed of Sound	$c_0 = 340 m/s$
acoustic constant	$b = 10^{-5} kg/(ms)$

List of Symbols

C_d	drag coefficient	
d_p	diameter of particle	m
E_{coh}	cohesive energy	W
E_{coll}	collision energy	W
E_{sou}	sound energy	W
e	coefficient of restitution	
F_{pg}	volumetric particle-fluid interaction force	N
f	frequency	Hz
f_{ac}	acoustic force	N
f_B	Basset force	N
f_c	contact force	N
f_d	drag force	N
f_{Mag}	Magnus force	N
f_{Saff}	Saffman force	N
f_v	cohesive force	N
f_{vm}	virtual mass force	N
G	shear modulus	Pa
g	gravity acceleration	m/s
Ha	Hamaker constant	J
h	bed height	m
I	moment of inertia	kg/m^2
K_n	normal elastic constant	$N/(m^{\frac{2}{3}})$
K_t	tangential elastic constant	N/m
k	wave number	m
l	bed length	m
N_p	number of particles	
p	pressure	Pa
Re	Reynolds number	
Re_p	particle Reynolds number	s
s	distance between particle surface	m
T	torque	N/m
t	time	s
U	amplitude of the velocity associated with the sound wave	m/s
u	gas velocity	m/s
u_{ac}	acoustic velocity	m/s
u_{mf}	minimum fluidization velocity	m/s
V_p	particle volume	m^3
w	bed width	m
Y	Young's modulus	Pa

Greek letters

α	attenuation coefficient	
β	fluid-particle inter-coefficient	kg/m^3s
γ_n	normal viscoelastic damping constant	Ns/m
γ_t	tangential viscoelastic damping constant	Ns/m
δ	displacement	m
δ_n	normal overlap	m
δ_t	tangential overlap	m
ε_p	porosity	
ε_g	concentration of particles	
κ	bulk modulus	Pa
μ_s	sliding friction coefficient	
μ_g	gas viscosity	Pas
ν	Poisson ratio	
ρ_p	particle density	kg/m^3
ρ_g	gas density	kg/m^3
τ	viscous stress tensor	s
ω	angular frequency	$1/s$

Subscripts

n	normal direction
p	particle
t	tangential direction
w	wall
x	x direction
y	y direction

Chapter 1

Introduction

Fluidization is a process which solid particles are converted from static solid-like state to dynamic fluid-like state by blowing fluid upwards through the solid-filled reactor. The fluidized bed is one of the best known contacting methods used in industry for fluidization process. A fluidized bed consists of fluid-solid mixture that exhibits fluid-like properties, which is widely used in energy, environmental and petrochemical industries due to their adaptability and prominent processing ability. Nowadays, fluidized beds are used for cooling, drying or heating in food processing industry, catalytic gas phase reactions or gas-solid reactions in chemical processing industry and pneumatic transport of powder. Fluidization provides advantages of increasing flowability and homogeneity, as well as way for bulk solid handling, allowing industries being able to design many processes which are otherwise not feasible. There are several types of fluidized beds with different usages, including stationary or bubbling fluidized bed, circulating fluidized bed, vibratory fluidized bed, transport or flash reactor, annular fluidized bed and so on.

A simple structure of a fluidized bed reactor is shown in figure 1.1. At the initial state, large quantities of static solid particles are placed in the fluidized bed. The fluid phase flows into the bed from the bottom inlet, making solid particles floating in fluid flow, which leads for particles to behave with fluid-like properties.

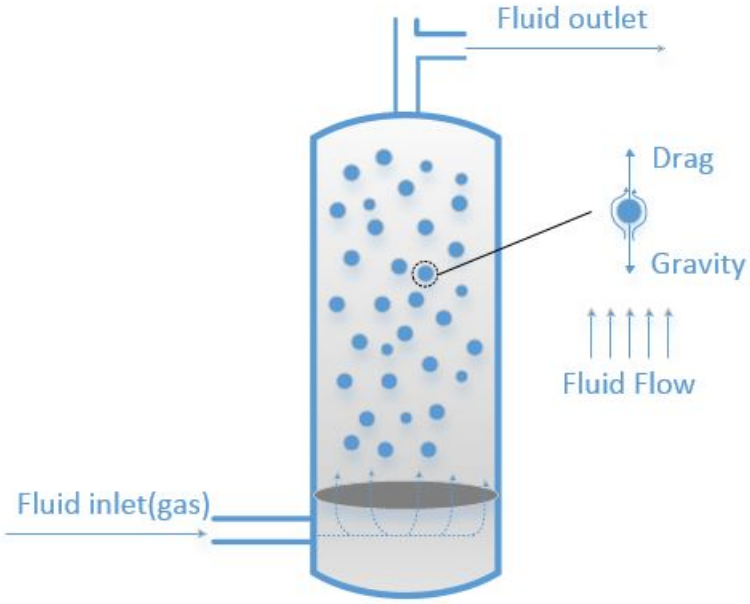

FIGURE 1.1: A schematic of a fluidized bed

It could be easily found that the full flow consists of a two phase of fluid-solid mixture from figure 1.1, while the fluid-solid mixture exhibits fluid-like properties in a fluidized bed reactor. For the gas phase, when it comes into the FBR (Fluidized Bed Reactor), the solids and fluid exert a "drag" force on each other. Once the solid particles are fluidized, the fluidized bed behaves differently as velocity increases [1]. When the inlet velocity is at a certain range of low velocity, the bed only suffers a few vibrate, while the height of the bed still remain almost the same as the original height. As the gas velocity increases, a point is reached where the drag force exerted on the particles equals the weight of the particles, which is called minimum fluidization with the corresponding velocity named minimum fluidization velocity. As the gas velocity increases beyond this minimum velocity, the particles are lifted higher whereas the bed porosity increases with it.

If the velocity increases further, bubbles would formate and set in the fluidized bed system. At even higher velocities, the bed can be further characterized by a slugging regime, and subsequently a turbulent regime.

The fluidization behavior also depends on the density and size of the solid particles. Small particles with a low density are more easily fluidized than large and heavy particles, as the gravity acting on the latter type is illatively much larger. The particle-particle interaction forces are relatively more important for small particles in comparison with those forces acting on large particles, causing small particles to exhibit a certain range of homogeneous expansion. Geldart classified particles into four different powder types, which are categorized as following [1, 2]:

1. Group A: Group A is defined as a group of materials who have a small mean size($d_p < 30\mu m$) and/or a low particle density($\rho_p < 1.4g/cm^3$), which fluidize easily, with smooth fluidization at low gas velocities without the formation of bubbles. When the gas velocity is higher, a point is eventually reached when bubbles start to form and the minimum bubbling velocity, which is always grater than the minimum fluidized velocity. Fluid cracking catalysts typically are in this category.

2. Group B: Group B contains most materials in the mean size and density ranges $40\mu m < d_p < 500\mu m$,$4g/cm^3 > \rho_p > 1.4g/cm^3$, sand being the most typical powder. For these particles, once the minimum fluidization velocity is exceeded, the excess gas appears in the form of bubbles, while these bubbles of group B particles can grow into a vary large size. Glass beads and corase sand are in this category.

3. Group C: Group C is designated as 'cohesive' particles, or very fine powders. The size of a typically group C particle is usually less than 30 μm, and it is extremely difficult to fluidize the particles of group C since the interparticle forces of these particles are relaticely large when compared to those resulting from the action of gas. Talc, flour and starch are in this category.

4. Group D: Group D contains materials who are either very large or very dense. Particles of this group is difficult to fluidize in deep beds. When gas velocity increase, a jet can be formed in the bed and materials of this group may be blown out with the jet in a spouting motion. If the gas distribution is uneven, spouting behavior and severe channeling can be expected. Roasting coffee beans and some roasting metals are in this category.

It is clear and easy to use Geldart's classification by Geldart diagram as displayed in Figure 1.2 for fluidization at ambient conditions and for u less than about 10 u_{mf}. Any kind of material with a known density ρ_p and mean size d_p could be classed by the diagram as expected.

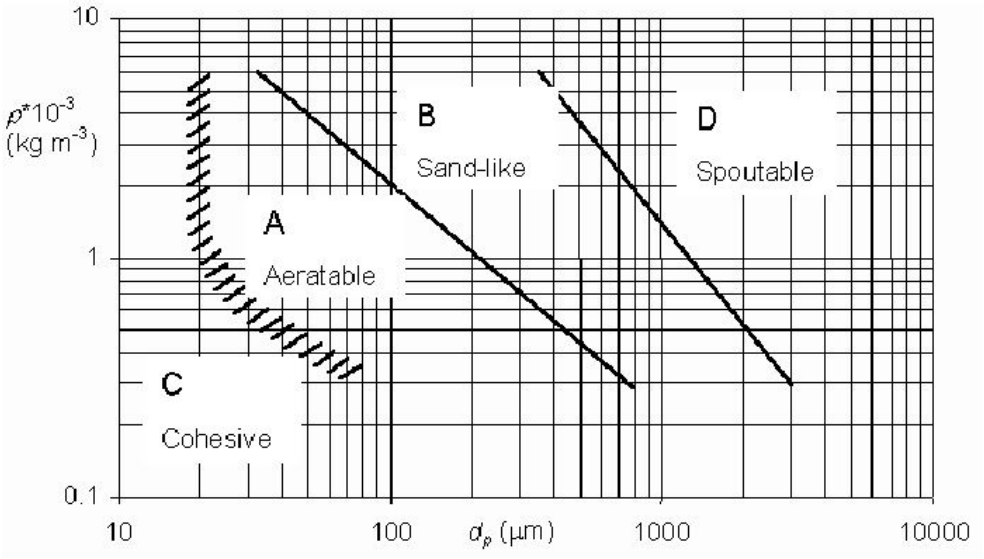

FIGURE 1.2: Geldart classification diagram

1.1 Agglomeration

Under dry conditions, fluidized beds with Geldart A/C particles encounter a severe agglomeration problem. For these fine particles, the cohesive force between particles is not able to be neglected, which would leave the particles tend to agglomerate with each other, and thus cast an important effect on the particle motions in the FBR processes. For example, when the solid begins to bind, the exchange area decreases and the properties of the two phases may be influenced, even the whole reaction maybe interrupted in this case.

For ultrafine particle fluidizations, the size of agglomerates attracts researchers attention since the particle motions suffer a lot with the phenomenon of agglomeration, and thus how to reduce the agglomeration becomes the first consideration of the researches during the past several decades. Researchers have paid more and more attention on the adaption of fluidized bed technology by using a variety of methods such as vibration, sound assistance and magnetic force are applied to enhance fluidization quality of ultrafine cohesive particles [3].

A vibrated fluidized bed has been applied for the fluidization of agglomerative particles with cohesive force [4, 5], which are difficult to be fluidized with a simple FBR. Some researchers have studied the vibrated fluidized bed since the late of 20th century and it is found that when the vibration is added to the particle bed, the minimum fluidization velocity becomes smaller [6].

An oscillating magnetic field applied to a FBR was studied firstly by Yu et al. [7], it was found that with the aid of an oscillating magnetic field at low frequencies, the bed of nanoparticle agglomerates can be smoothly fluidized with the minimum fluidization velocity reduced significantly.

An electric-field enhanced fluidized bed was studied by Willigen et al. [8] by simulations and it was found that the electric fields reduce bubble size in electric-field enhanced fluidized beds: at moderate field strengths, the macroscopic behavior is not strongly modified while at very high field strength, the particles form visible strings throughout the bed and only show little free movement. Also, the electric-field distribute gas into small bubbles in the bottom of the bed and decrease the coalescence rate, which helps a smaller bubble size.

An acoustic fluidized bed means to apply acoustic waves on a FBR, while the sound wave, it was found that applying sound waves helps to disrupt the large cluster of particles [9] and the agglomerate size tends to change its properties when applying different kinds of sound waves with varieties of parameters of acoustic fields [3].

Those methods of adding different types of signals on the FBR have their own advantages and shortages, while vibrated fluidized bed is energy-saving but not stable since it may distroy the particle stucture, which also leaves a severe impact on the motion of the system; the oscillating magnetic assisted fluidized bed is easier to generated by current source but magnetic and nonmagnetic may behave different when adding magnetic field; The electric-field fluidized bed requires certain field strength, which is not easy to maintain; the sould assisted fluidized fluidized bed is stable, with all properities such as intensity and frequency easy to control although the range maybe too large and difficult to decide. Also, sound waves-used as an alternative excitation method is more inexpensive, affects the entire particle bed, does not require any physical contact between sound generator and nanoparticles. For those reasons, sound-assisted fluidized bed technology is studied.

1.2 State-of-the-art Research

In this project, the adaptation of adding an acoustic wave onto the fluidized bed is studied, for which the basic models are introduced in the later chapter. In this section, the results of researchers about sound-assisted fluidized beds are introduced to have a better understand of current studies.

It has been introduced before that a sound-assisted fluidized beds help to disrupt large clusters of particles, which means the agglomerates becomes smaller when adding acoustic waves onto the system, more detailed experiments and CFD simulations are done by many researchers to figure out the effects of adding different kinds of acoustic fields, which are summarized below.

Morse [10] studied the use of sonic energy as a means for overcoming the tendency for granular material to pack by experiment and found that low frequency and high sonic energy will markedly improve the fluidization of nonfluent, fine-grained powders, while in other conditions intense channeling or slugging would appear rather than fluidization. The influence of the acoustic waves frequency on a sound-assisted fluidized bed is studied by Russo et al. [11], who focous on sound-assisted fluidization of nonfluent catalyst particles with a 145mm column and the pressure level of sound field from 110 to 140 dB, the frequency varing from 30 to 1000Hz . In the experimental section, they also determined that for given weight and sound pressure level, the ranges of frequency within which channel-free homogeneous fluidization coud be obtained, which means that channeling would be found when frequency is above or below the certain range.

Homogeneous fluidization could be obtained in sound-assisted operation of beds of micro particles such as 11μm-sized zeolitic catalyst, 8μm-sized ash and 5μm-sized talc [9, 12]. However, the homogeneous can be disrupted by instable conditions with the appearance of bubbles [13]. Levy et al. [9] studied the effect of an acoustic field on bubbling in a gas fluidized bed and presents the combined effects of gas velocity and frequency and intensity of the sound waves on bubbling behavior and got data on minimum bubbling velocity, bubbling frequency and bed expansion in a shallow batch fluidized bed at room temperature by experiments. It is found that at natural frequency of the bed, high intensity sound waves resulted in the reductions in both the minimum bubbling and minimum fluidization velocities; while

increasing sound level causes a decrease in bed expansion and an increase in bubble frequency. Futhermore, Herrera and Levy [14] studied the bubbling characteristics of sound-assisted fluidized beds and found that high intensity sound disrupted the cohesive nature of the powders, allowing both homogeneous and bubbling fluidization, with data shows that the minimum bubbling velocity is affected by the sound pressure level, which indicates that the bubbling characteristics could be controlled by the value of the sound pressure level. Later on, Herrera and Levy [15] also set up an acoustic standing-wave theory which assumes that the bed behaves as a 1D, quasi fluid with constant speed of sound to model the sound-pressure-level data. The comparison between the theory and the experimental data indicates good agreement, which means that sound wave transmission through a column could be treated as a standing wave.

For all studies mentioned above, they mostly focus on a micron- or submicron-scales, while for nanoparticles, it was found that nanoparticle agglomerates can be smoothly fluidized if the gas velocity is increased far above the minimum fluidization velocity of primary nanopartilces with a much-reduced fluidizing gas velocity, hardly any elutriation of the nanoparticles was observed [16]. Zhu et al. [17] thus presents some observations on the effects of sound on the fluidization behavior of the nanoparticle agglomerates, which shows that with the aid of sound wave excitation at low grequencies, the bed of nanoparticle agglomerates can be fluidized and the minimum fluidization velocity is reduced. In addtion, they also find that under the influence of sound, channeling of the bed quickly disappered and the bed expands uniformly, which means that the bed expansion and bubble characteristics are strongly dependent on the sound frequency and sound pressure level, while sound cast almost no impact on the fluidizaion when the frequency of the sound is extremely high, such as above 2000 Hz.

Also, Guo et al. [18] studied the fluidization behavior of nanoparticles (5-10 nm SiO_2) and found out that sound wave erergy has a significant influence on the compact ratio of a packed bed and the bed of nanoparticle agglomerates can be fluidized smoothly with the assistance of an acoustic field by experimental results. Later on, Guo et al. [3] also studied three different types of SiO_2 ultrafine particles to investigate the fluidization behavior in a fluidized bed with sound excitation, which shows that the agglomerate size tends to reduce with an increase in sound pressure level and the existence of a critical sound frequency, while the agglomerate size is decreased with increasing sound frequency as sound frequency less than critical sound frequency. Moreover, some additional experiments were done [19], which shows that the minimum fluidization of the particles could be achieved when operated in an acoustic field with appropriate combinations of bet weight and sound intensity and frequency [20]. Later, they also studied the flow characteristis in a high temperature fluidized bed with sound assistance [21].With the conclusions that the at a given sound pressure level, there exists a minimum value of the minimum fluidization velocity, which corresponds to a good fluidization quality. Another similar research of the pressure fluctuation of the particles has also been studied by Si et al. [22], whose results also showed that the minimum fluidization velocity has a minimum value with a certain frequency of sound wave.

Simple particles are discussed by large quantities of researchers, the study of mixtures also attracts researchers, while Si and Guo [23] studied the fluidization characteristics of binary mixtures of particles with biomass(sawdust and wheat stalk) and quartz sand in an acoustic bubbling fluidized bed and it is found by experiments that the addition of quatz sand can improve the fluidization quality of biomass. The minimum fluidization velocity of the mixtures increased with the increasing of biomass content in the mixtures while the minimum fluidization velocity decreased

with the ncreasing of sound pressure level and had a minimum value over a vertain found frequency range. Ammendola et al. [24] also studied a binary mixture of two oxides, Al_2O_3 and Fe_2O_3 and it is found that the fluidization of this binary mixture varies with the amount of the two powders, while the addition of Fe_2O_3 has a beneficial effect on the fluidization quality of the binary mixtures.

All the results mentioned above are done through experiment at studies, while theoretical investigation and numerical methods could also help to solve problems. Wang et al. [25] studied the effects of sound pressure level and sound frequency applied on a fluieized bed by means of discrete element method(DEM) and found that computed granular temperature is increased with the increase of sound pressure level and the acoustic force increases firstly and later decreases after reaching maximum with the increase of sound frequency. The research made a useful conclusion about the relationship between sound pressure level, sound frequency and the fluid field characteristic.

Since fluidized beds perform well in heat recovery processes due to its rapid mixing property, they are widely used in a variety industries and thus the heat transfer properties are also important to be discussed. Wankhede et al. [26] studied the heat transfer for different sized particles at different acoustic conditions, gas velocities and angular positions around the circumference of heat transfer surface and found out the optimum fluidization velocities and acoustic conditions to obtain maximum heat transfer rates from the heat transfer surface to the certain bed material. They also studied the heat transfer between a bubbling fluidized fluidized bed of fine powders with an immersed heating surface in absense and presence of acoustic waves and it is found that heat transfer rates could be improved by the ocsillation of the particles at certain frequencies while the location for maximum heat transfer rates was at the sides of the tube and shifted upward at higher gas velocities.

1.3 Objectives of the Present Work

In this study, the main objective is to model the agglomeration phenomenon and investigate what effects acoustic waves could cast on the particle agglomerates by comparing the flow behavior of fine cohesive particles in a normal fluidized bed and a sound-assisted fluidized bed. Simulation results of non-cohesion case, cohesive case and sound-assisted case are performed for fine particles(with a diameter of $20\mu m$, corresponding to group A particles). In case of as well as larger particles(with a diameter of $1mm$, corresponding to group B particles) in case of computational limits of software when the size of particle is relatively small. By analyzing the pressure drop, bed height, instantaneous snapshots, bubble size, agglomeration size and vector plot of velocity, the phenomenon of agglomeration and how acoustic waves help to break particle agglomerates are investigated.

Chapter 2

Numerical Methods

2.1 CFD Multiscale Models

Computational fluid dynamics(CFD) is a fluid mechanics tool that uses numerical analysis and data structures to solve and analyze problems related to fluid flows. The basic idea of CFD is to consider how to solve continuous flow problems using discrete models. One of the simple methods is to divide fluid fields into tiny elements and apply certain suitable algorithm(Lagrangian or Eulerian approach or so on) in order to analyze the moving trajectory on each element. With the help of computers, better solutions could be achieved.

To be more in detail, there are several models to solve the motion of two-phase flows. One of the classifications of these models is according to the scales. The difficulty and complexity of two-phase flow is mainly due to the large separation of scales. For example, micro-scale models collect the motion of each simple particle and element, while macro-scale models collect the information of fluid flow and gas motion. Thus Van der Hoef et al. [27] divide all simulation methods into five classes according to its scales, which is shown as below:

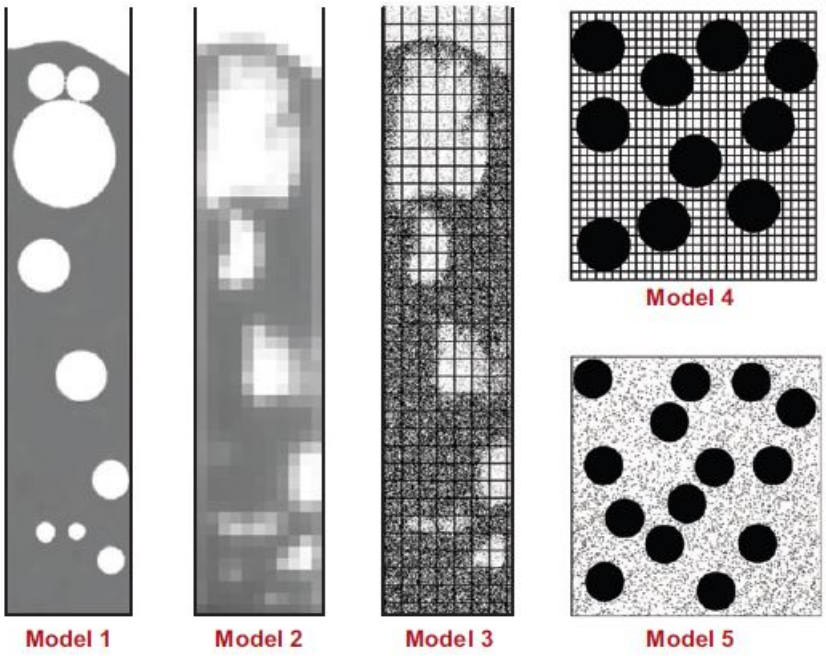

FIGURE 2.1: Classification of gas-solid flow models[27]

1. discrete bubble model: it regards the fluid motion as many discrete bubbles and uses a Lagrange algorithm to solve the motion of gas phase and regards solid

	Name	Gas phase	Solid phase	Gas-solid coupling	Scale
1.	Discrete bubble model	Lagrangian	Eulerian	Drag closures for bubbles	Industrial (10 m)
2.	Two-fluid model	Eulerian	Eulerian	Gas-solid drag closures	Engineering (1 m)
3.	Unresolved discrete particle model	Eulerian (unresolved)	Lagrangian	Gas-particle drag closures	Laboratory (0.1 m)
4.	Resolved discrete particle model	Eulerian (resolved)	Lagrangian	Boundary condition at particle surface	Laboratory (0.01 m)
5.	Molecular dynamics	Lagrangian	Lagrangian	Elastic collisions at particle surface	Mesoscopic (<0.001 m)

FIGURE 2.2: Classification of the various models used for simulating dense gas-solid flow in the context of gas-fluidization[27]

phase to be continuous to get the motion model. Bubble motion model is often gain by conclusions of experiments.

2. two-fluid model, it regards the solid particles as continuous fluid phase and analyze the motion similar to gas phase, using Euler algorithm to describe mass, momentum and energy balance equation.

3. unresolved discrete particle model, the solution of gas phase and solid phase need to be analyze separately in the scale of mesh and particle. The motion of gas phase is solved using an Euler algorithm, while the motion of the solid phase is solved using a Lagrange algorithm. A famous representative of this method is Computational Fluid Dynamics-Discrete Element Method(CFD-DEM).

4. resolved discrete particle model, the motion of solid phase is solved using a Lagrange algorithm, while the motion of gas phase is solved using a Euler algorithm. Moreover, the mesh scale of this method is smaller than the particle scale, which makes the solution to fluid motion more accurate. However, the mesh number is quite large, which requires more computational resources.

5. molecular dynamics, the motion of solid phase is solved using a Lagrange algorithm, while the motion of gas phase is solved on the base of the motion of a single molecular. By analyzing the force suffered by a single molecular, the motion of gas phase could be obtained, which also requires large quantities of computational resources.

2.2 CFD Model

The Discrete Element Method(DEM), which can resolve particle flow behaviors at an individual particle level, has been widely used for studying granular-fluid flow in fluidized-bed systems [28]. CFD-DEM model is a process used to model or simulate systems combining fluids with solids or particles.

Using CFD-DEM method, the two components of the system, gas phase and solid phase are modeled separately, including particle motions and fluid flows, from which solving governing equations could simulate the behavior of fluidized beds.

2.2.1 Governing Equations

Different CFD models have been used in varieties of cases, while Z.Y. Zhou et al. [29] discussed three sets of formulations existing in the CFD-DEM approach. In this project, combined with the software, only set II is used and introduced and could be written as:

$$\frac{\partial \varepsilon_g}{\partial t} + \nabla \cdot (\varepsilon_g \boldsymbol{u}) = 0 (mass - conservation) \tag{2.1}$$

$$\rho_g \varepsilon_g [\frac{\partial (\boldsymbol{u})}{\partial t} + \nabla \cdot (\boldsymbol{uu})] = -\varepsilon_g \nabla p - \boldsymbol{F}_{pg} + \varepsilon_g \nabla \cdot \tau + \rho_g \varepsilon_g \boldsymbol{g} (momentum - conservation) \tag{2.2}$$

Where $\boldsymbol{F}_{pg} = \frac{1}{\Delta} \sum_{i=1}^{n} (\boldsymbol{f}_{d,i} + \boldsymbol{f}_i^{''})$ stands the volumetric particle-fluid interaction force, with $\boldsymbol{f}_{d,i}$ representing the drag force and $\boldsymbol{f}_i^{''} = \boldsymbol{f}_{vm,i} + \boldsymbol{f}_{B,i} + \boldsymbol{f}_{Saff,i} + \boldsymbol{f}_{Mag,i}$ is the sum of particle-fluid interaction forces on particle i, other than the drag, pressure gradient and viscous forces which are the domaint forces in particle-fluid flow [29]. τ represents the viscous stress tensor and writes $\tau = \mu[\nabla \boldsymbol{u} + (\nabla \boldsymbol{u})^{-1}] - \frac{2}{3}\mu(\nabla \cdot \boldsymbol{u})\boldsymbol{\delta}_k$ for Newtonian fluids.

The set of model corresponds to hydrodynamic models A, which have been used in a variety of two-phase flows. If the pressure only attributes to the fluid phase, model B is referred, otherwise model A is referred. Thus model A consistent with set II and model B with the other two sets.

2.3 DEM Models

2.3.1 Governing Equations

The present interest is focused on the particle behavior instead of fluid phase, thus the CFD cell is determined at a large scale, [29] while each cell may contain many particles.

For the motion of solid phase, the basic idea to solve it is to apply Newton's second law on each particle and analyze the force the particle suffers. The equations are given by [30, 31]:

$$m_i \frac{d\boldsymbol{v}_{p,i}}{dt} = \sum_j (\boldsymbol{f}_{c,ij}^n + \boldsymbol{f}_{c,ij}^t) + \sum_k \boldsymbol{f}_{v,ik} + \sum_w (\boldsymbol{f}_{c,iw}^n + \boldsymbol{f}_{c,iw}^t + \boldsymbol{f}_{v,iw}) + \boldsymbol{f}_{pg,i} + m_i \boldsymbol{g} \tag{2.3}$$

$$I_i \frac{d\boldsymbol{\omega_i}}{dt} = \sum_j \boldsymbol{T}_{t,ij} + \sum_w \boldsymbol{T}_{t,iw} \tag{2.4}$$

m_i,I_i,$\boldsymbol{v}_{p,i}$,$\boldsymbol{\omega_i}$ represent the mass, moment of inertia, translational velocity and rotational velocity of particle i. In the first equation, forces acting on the system are introduced: normal contact force $\boldsymbol{f}_{c,ij}^n$, tangential contact force $\boldsymbol{f}_{c,ij}^t$ from collision of two particles i and j, normal contact forces $\boldsymbol{f}_{c,iw}^n$ and tangential contact force $\boldsymbol{f}_{c,iw}^t$ from collision of particle i and wall, van der Waals force forces from the interactions $\boldsymbol{f}_{v,ik}$ between two particles i, k and $\boldsymbol{f}_{c,iw}$ between particle i and wall and gravitational force $m_i \boldsymbol{g}$. In the second equation, $\boldsymbol{T}_{t,ij}$ represents the torque acting on particle i due to particle, $\boldsymbol{T}_{t,iw}$ represents the torque acting on particle i from wall.

It should be noted that the item $\boldsymbol{f}_{pg}$, representing the particle-fluid interacting force, is the sum of total particle-fluid interaction force on an individual particle i, which could be written as $\boldsymbol{f}_{pf} = \boldsymbol{f}_{d,i} + \boldsymbol{f}_{\nabla p,i} + \boldsymbol{f}_{\nabla \cdot \tau,i} + \boldsymbol{f}_{vm,i} + \boldsymbol{f}_{B,i} + \boldsymbol{f}_{saff,i} + \boldsymbol{f}_{Mag,i}$.

2.3.2 Drag Force Models

By the method of dimensional analysis, drag force is known to be involved with four variables, which are: velocity u, fluid density ρ, viscosity ν, body size, usually in

terms of the frontal area A. When regarding drag force also as a part of the function with those variables, the equation could be written as:

$$f_a(f_d, u, A, \rho, \nu) = 0 \tag{2.5}$$

Applying the algorithm of the Buckingham π theorem, the components of the equation could be reduced into only two dimensionless parameters by combination as: drag coefficient C_d and Reynolds number Re, given by: $Re = \frac{u\sqrt{A}}{\nu}$ and $C_d = \frac{F_d}{\frac{1}{2}\rho A u^2}$. Thus the drag force equation is reduced to:

$$f_b(\frac{u\sqrt{A}}{\nu}, \frac{f_d}{\frac{1}{2}\rho A u^2}) = 0 \tag{2.6}$$

There are varieties of different correlations of drag force equations, of which DiFelice correlation, KochHill correlation, Schiller and Naumann correlation and Gidaspow correlation are the most famous and will be introduced in this section.

1. DiFelice drag model

DiFelice firstly proposed a continuous single-function correlation for the drag force by using an empirical fit to a wide range of fixed and suspended-particle systems covering the full practical range of particle Reynolds number Re_p and void fraction ε_g [19], for which the equations are given by:

$$f_{d,i} = \frac{1}{8} C_d \rho_f \pi d_p^2 (\boldsymbol{u}_g - \boldsymbol{v}_{p,i}) |\boldsymbol{u}_g - \boldsymbol{v}_{p,i}| \varepsilon_g^{-\chi} \tag{2.7a}$$

with

$$C_d = (0.63 + \frac{4.8}{\sqrt{Re_p}})^2 \tag{2.7b}$$

$$Re_p = \frac{\varepsilon_g \rho_g d_p |\boldsymbol{u}_g - \boldsymbol{v}_{p,i}|}{\mu} \tag{2.7c}$$

$$\chi = 3.7 - 0.65 exp[-\frac{(1.5 - log_{10} Re_p)^2}{2}] \tag{2.7d}$$

2. KochHill drag model

KochHillDrag model follows the correlation of Koch and Hill in 2001 based on lattice-Boltzmann simulations [32]:

$$f_{d,i} = \frac{V_p \beta (\boldsymbol{u}_g - \boldsymbol{v}_{p,i})}{\varepsilon_p} \tag{2.8a}$$

with

$$\beta = \frac{18 \mu_g \varepsilon_g^2 \varepsilon_p}{d_p^2} (F_0(\varepsilon_p) + \frac{1}{2} F_3(\varepsilon_p) Re_p) \tag{2.8b}$$

$$Re_p = \frac{\varepsilon_g \rho_g |\boldsymbol{u}_g - \boldsymbol{v}_{p,i}| d_p}{\mu_g} \tag{2.8c}$$

$$F_0(\varepsilon_p) = \begin{cases} \frac{1 + 3\sqrt{\frac{\varepsilon_p}{2}} + \frac{135}{64}\varepsilon_p ln(\varepsilon_p) + 16.14\varepsilon_p}{1 + 0.681\varepsilon_p - 8.48\varepsilon_p^2 + 8.16\varepsilon_p^3} & \varepsilon_p < 0.4 \\ \frac{10\varepsilon_p}{\varepsilon_g^3} & \varepsilon_p \geq 0.4 \end{cases} \tag{2.8d}$$

$$F_3(\varepsilon_p) = 0.0673 + 0.212\varepsilon_p + \frac{0.0232}{\varepsilon_g^5} \tag{2.8e}$$

3. Gidaspow drag model

Gidaspow model combines Ergun correlation and Wen-Yu correlation, which is shown below:

$$f_{d,i} = \frac{V_p \beta (\boldsymbol{u}_g - \boldsymbol{v}_{p,i})}{\varepsilon_p} \tag{2.9a}$$

with

$$\beta = \begin{cases} 150\frac{\varepsilon_p^2 \mu_g}{\varepsilon_f^2 d_p^2} + 1.75\frac{\varepsilon_p \rho_g}{\varepsilon_f d_p}|\boldsymbol{u}_g - \boldsymbol{v}_{p,i}|\varepsilon_f & \varepsilon_f < 0.8 \\ \frac{3}{4} C_d \frac{\varepsilon_p \rho_g}{d_p}|\boldsymbol{u}_g - \boldsymbol{v}_{p,i}|\varepsilon_f^{-2.65} & \varepsilon_f \geq 0.8 \end{cases} \tag{2.9b}$$

$$Cd = \begin{cases} \frac{24}{Re_p}(1 + 0.15 Re_p^{0.687}) & Re_p < 1000 \\ 0.44 & Re_p \geq 1000 \end{cases} \tag{2.9c}$$

$$Re_p = \frac{\varepsilon_f \rho_f d_p |\boldsymbol{u}_g - \boldsymbol{v}_{p,i}|}{\mu_g} \tag{2.9d}$$

2.3.3 Collision Models

For the term of contacting force between particles, the collision model needs to be concerned, while two kinds of models are mostly used: soft sphere model and hard sphere model and in this case, soft sphere model is used.

The soft sphere model, as figure 2.3 shows, was introduced by Cundall and Strack in 1979, considers the interaction between particles and allows the particles to overlap slightly [11], which applies spring-damp system to simulate the motion properties between particles.

When calculating the contact force between particles, different contact models come out, which are discussed below:

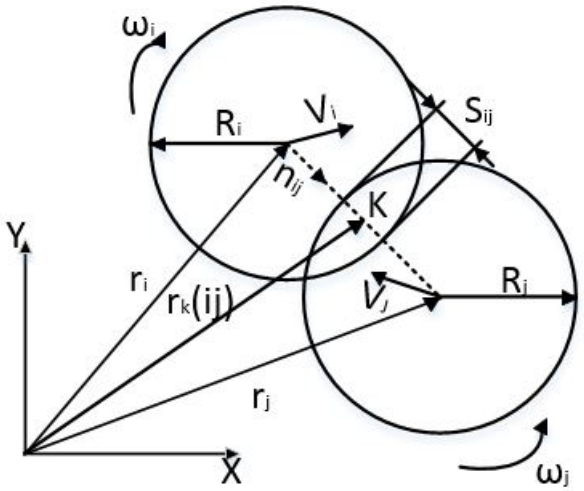

FIGURE 2.3: Scheme of soft sphere model

1. hertz contact model

Suppose the radius of two particles are R_1 and R_2, similarly, mass as m_1 and m_2, Young's modulus as Y_1 and Y_2, shear modulus as G_1 and G_2, e as the coefficient of resitution and ν the possion ratio. The force between two particles could be calculated by:

$$F = (K_n \delta n_{ij} - \gamma_n v_{ij}) + (K_t \delta t_{ij} - \gamma_t v_{ij}) \tag{2.10a}$$

with

$$K_n = \frac{4}{3}Y^*\sqrt{R^*\delta_n} \tag{2.10b}$$

$$\gamma_n = -2\sqrt{\frac{5}{6}}\beta\sqrt{S_n m^*} \geq 0 \tag{2.10c}$$

$$K_t = 8G^*\sqrt{R^*\delta_n} \tag{2.10d}$$

$$\gamma_t = -2\sqrt{\frac{5}{6}}\beta\sqrt{S_t m^*} \geq 0 \tag{2.10e}$$

$$S_n = 2Y^*\sqrt{R^*\delta_n}, S_t = 8G^*\sqrt{R^*\delta_n} \tag{2.10f}$$

$$\beta = \frac{ln(e)}{\sqrt{ln^2(e)+\pi^2}} \tag{2.10g}$$

$$\frac{1}{Y^*} = \frac{(1-\nu_1^2)}{Y_1} + \frac{(1-\nu_2^2)}{Y_2}, \frac{1}{G^*} = \frac{2(2-\nu_1)(1+\nu_1)}{Y_1} + \frac{2(2-\nu_2)(1+\nu_2)}{Y_2} \tag{2.10h}$$

$$\frac{1}{R^*} = \frac{1}{R_1} + \frac{1}{R_2}, \frac{1}{m^*} = \frac{1}{m_1} + \frac{1}{m_2} \tag{2.10i}$$

with δ_n and δ_t the normal and tangential overlap distance between 2 particles, K_n and K_t the elastic constant for normal and tangential contact, γ_n and γ_t the viscoelastic damping constant for normal and tangential contact.

2. hooke contact model

The contact force between two particles could also be expressed by hooke contact model, which writes as:

$$F = (K_n\delta n_{ij} - \gamma_n v_{ij}) + (K_t\delta t_{ij} - \gamma_t v_{ij}) \tag{2.11a}$$

with

$$K_n = \frac{16}{15}\sqrt{R^*}Y^*(\frac{15m^*V^2}{16\sqrt{R^*}Y^*})^{\frac{1}{5}} \tag{2.11b}$$

$$\gamma_n = \sqrt{\frac{4m^*K_n}{1+(\frac{\pi}{ln(e)})^2}} \geq 0 \tag{2.11c}$$

$$K_t = K_n \tag{2.11d}$$

$$\gamma_t = \gamma_n \tag{2.11e}$$

2.3.4 Cohesive Models

The cohesive force is mainly decided by van der Waals force, whose magnitude between particles i and j is modeled by [30]:

$$F_{vdw}(A,s) = \frac{A2r_i r_j(r_i+r_j+s)}{3s^2(2r_i+2r_j+s)^2}[\frac{s(2r_i+2r_j+s)}{(r_i+r_j+s)^2-(r_i-r_j)^2} - 1]^2 \tag{2.12}$$

where A is the Hamaker constant and s the distance between particle surfaces. For different group of particles, Hamaker constant differs and depends on the property of material. It is assumed that there exists a minimum and maximum distance s_{min} and s_{max}, when the distance s is larger than s_{max}, the van der waals force will not be considered, when the distance is smaller than s_{max}, the van der waals force equation is given by equation 2.13 as figure 2.4 illustrates:

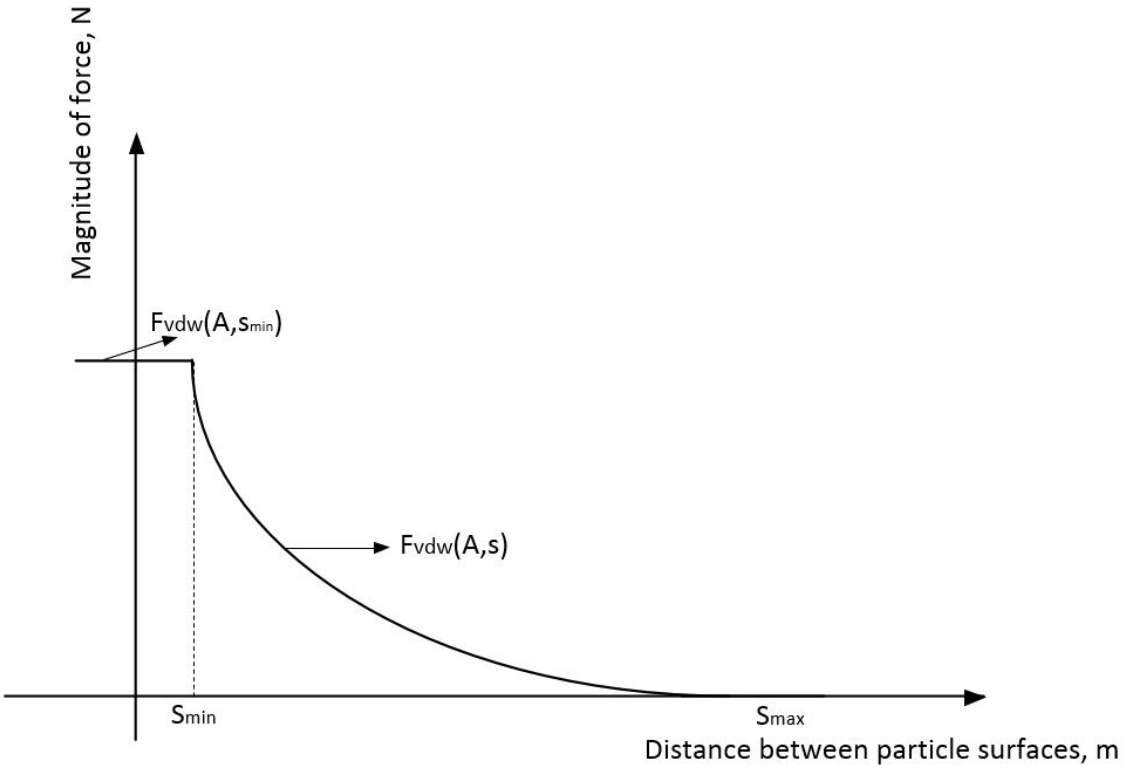

FIGURE 2.4: Scheme of soft sphere model

$$\boldsymbol{f}_{v,ij} = \begin{cases} -F_{vdw}(A,s)\boldsymbol{n}_{ij} & s_{min} < s < s_{max} \\ -F_{vdw}(A,s_{min})\boldsymbol{n}_{ij} & s \leq s_{min} \end{cases} \tag{2.13}$$

with $s_{max} = \frac{r_i + r_j}{4}$ and s_{min} corresponded to the inter-molecular spacing [30].

For the van der Waals force between particle and wall, the wall could be considered as a particle whose radius is much larger than the other particles, and thus the equation could be simplified into:

$$\boldsymbol{v,iw} = -f_{v,iw}\boldsymbol{n}_{iw} = \begin{cases} -\frac{Ar_p}{6s^2}\boldsymbol{n}_{iw} & s_{min} < s < s_{max} \\ -\frac{Ar_p}{6s_{min}^2}\boldsymbol{n}_{iw} & s \leq s_{min} \end{cases} \tag{2.14}$$

2.4 Acoustic Theory

Basically, acoustic field theory is related to the description of sound waves, which derives from fluid dynamics. Sound waves in a fluid could be modeled as an equation of mass balance(continuity) and momentum balance, which is shown as below:

$$\frac{\partial p}{\partial t} + \kappa \nabla \cdot u = 0 \tag{2.15}$$

$$\rho_0 \frac{\partial u}{\partial t} + \nabla p = 0 \tag{2.16}$$

with the equation (2.16) the mass balance equation and (2.17) the momentum balance equation.

When applying an acoustic field on the fluidized bed, several assumptions are often made to model the energy balance of agglomerates in an acoustic fluidized bed [3]:

(1)the formed agglomerates are spherical with the same size;

(2)the wall effect is neglected;

(3)the van der Waals force is predominant by compared with other inter-particle force.

The energy balance equation is thus given by:

$$E_{coll} + E_{sou} = E_{coh} \tag{2.17}$$

Which means that the sum of collision energy and sound energy equals cohesive energy. To be simplified, when applying sound wave onto a fluidized bed, it could be regarded as a sine wave with a certain amplitude, with could be written as sound pressure level(SPL), which could be determined by the equation (2.18)(Assuming that the sound propagates as a plane wave in an unbounded and solids-air space as a first approximation) [33]:

$$SPL = 20log\frac{U}{\sqrt{2}U_{ref}} \tag{2.18}$$

where U_{ref} represents the reference velocity whose value is $4.83 \times 10^{-6} cm/s$ and U the amplitude of the velocity associated with the sound wave.

To be more in detail, it could be assumed that the application of the acoustic field induces an oscillatory component of gas velocity $Usin(2\pi ft)$ due to sound, where f is the frequency of the acoustic field and U is the amplitude of the oscillating gas velocity, which could be derived from Equation(2.19) [34]. It is assumed that the local gas velocity and acoustic velocity has the relationship:

$$u_{ac}(x,t) = Usin(2\pi ft - kx)e^{-\alpha x} \tag{2.19}$$

with the wave number in the medium k a function of sound frequency, $k = \frac{2\pi f}{c_0}$ and α the attenuation coefficient, $\alpha = \frac{2b(\pi f)^2}{(\varepsilon_s\rho_s+\varepsilon_g\rho_g)c_0^3}$, where c_0 is the sound speed of the acoustic medium (air) and b is a constant.

The existence of acoustic wave in a fluidized cast a force acting on a particle, which also induces an oscillatory component of gas velocity and the acoustic force model is given by the equation below, which is proposed by Urciuolo et al. [35] and Russo et al. [11]:

$$\boldsymbol{f}_{ac} = \frac{\beta_{UR}V_p}{1-\varepsilon_g}(u_{ac} - v_p) \tag{2.20}$$

$$\beta_{UR} = \frac{3C_d\rho_g(1-\varepsilon_g)|u_{ac} - v_p|}{4d\rho_s V_p} \tag{2.21}$$

where the term u_{ac} is the velocity of gas with the influence of acoustic field and $u_{ac} - u_p$ is slip velocity between gas and particle velocity due to sound wave which could be calculated by Equation(2.10), β_{UR} is the fluid-particle inter coefficient.

Chapter 3

Validation

3.1 Case Introduction and Model Settings

The numerical model is firstly validated with a simple case of fluidization of fine particles, the results of which are compared with the results reported by Y.Gu et al. [30]

The computation domain and boundaries and mesh grids are illustrated in figure 3.1, with the geometric dimensions and the physical properties are used as the same as those from the reference paper.

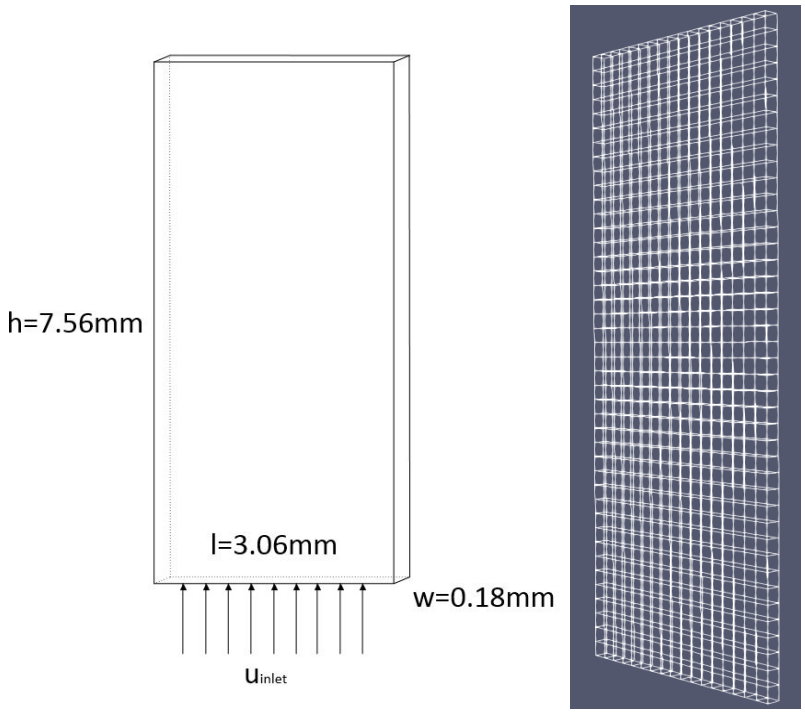

FIGURE 3.1: Computation domain and boundaries with the wire frame of mesh

The domain area is a cuboid with length 3.06mm, width 0.18mm and height 7.56mm, consisting a pseudo-2D fluidized bed. The cell size of each mesh element is set to be equal to the width of the cuboid domain as $\delta x = \delta y = \delta z = 0.06mm$ and thus the whole region is divided into $18 \times 1 \times 42 = 756$ grids, for which the mesh grid is also shown in figure 3.1.

For the solid phase, the main material properties are also taken from the same literature, which are shown in Table 3.1. Particle with diameter $60\mu m$ and density 2250 kg/m^3 is selected, which corresponds to group A particles as introduced in

chapter 1 and thus the Hamaker constant of 2.1×10^{-21} is chosen. As for Young's modulus, there are three values in the paper, $7 \times 10^{10} Pa$, $10^8 Pa$, and $10^6 Pa$. For the reason that the software require Young's modulus in SI unit larger than $5 \times 10^6 Pa$ and smaller than $1 \times 10^9 Pa$, the Young's modulus value chosen in this part is $10^8 Pa$.

For the gas phase, the dynamic viscosity μ_g is set to be $1.81 \times 10^{-5} Pa \cdot s$, with gas density $\rho_g = 1.205$, thus the kinematic viscosity is calculated by $\nu_g = \frac{\mu_g}{\rho_g} = 1.5 \times 10^{-5} m^2/s$.

For the chosen of DEM time step, since the main region mesh grid size are relatively small, a computing time step of 0.000001s is chosen and coupling interval 100, with the CFD time step 0.0001s.

TABLE 3.1: Parameters of the case simulation

parameter	value	unit
Gas density ρ_g	1.205	kg/m^3
Gas dynamic viscosity μ_g	1.81×10^{-5}	$Pa \cdot s$
Gravity g	9.81	m/s^2
Number of particles N_p	9522	-
Particle density ρ_p	2250	kg/m^3
Young's modulus Y	10^8	Pa
Poisson's ratio ν	0.22	-
Restitution coefficient e	0.94	-
Sliding friction coefficient μ_s	0.18	-
Gas inlet velocity u_g	0.02	m/s
Geometry(width,depth,height)	$3.06 \times 0.18 \times 7.56$	mm
Cell size(width,depth,height)	$0.18 \times 0.18 \times 0.18$	mm
Particle diameter d_p	60	μm
Simulation time of CFD t	1×10^{-4}	s
Simulation time of DEM t_{DEM}	1×10^{-6}	s
coupling interval n	100	-

The simulation is generally based on three softwares: solid phase via LIGGGHTS, fluid phase via OpenFOAM and coupling of two phases via CFDEM.

In CFD settings, firstly, the boundary conditions need to be determined and only 4 parameters: pressure p, density ρ, velocity u, voidfraction ε_g are considered in this case, with the details of boundarty settings shown in table 3.2.

TABLE 3.2: Settings of boundary conditions

parameter	inlet	outlet	walls
density ρ	internalField uniform 1.205, boundary conditions zeroGradient		
velocity u	uniformFixedValue	zeroGradient	zeroGradient
pressure p	zeroGradient	fixedValue, uniform 0	zeroGradient
voidfraction ε_g	fixedValue, uniform 1	fixedValue, value uniform 1	zeroGradient

The value of inlet velocity needs to be set as uniformFixedValue since the inlet velocity needs to change with time, of which the value is set to be (0 (0 0 0))(0.005 (0 0 0.02)) which means that the inlet velocity is 0 at the beginning and will increase to 0.02m/s after 0.005s.

Secondly, the constant parameters are considered, including the settings of gravity, coupling properties settings and transport properties. As mentioned in Chapter 2 before, the forces that fluid phase suffers are: $-\varepsilon_g \nabla p_g$, representing pressure gradient force, corresponds to forceModel-gradPForce command in CFDEM coupling; $\nabla \cdot \tau_g$, representing force due to fluid stress tensor, corresponds to forceModel-viscForce command in CFDEM coupling; $\boldsymbol{F}_{pg}$, representing the interaction force and mainly only drag force is considered in this case, corresponds to dragForce models in CFDEM couplings; the forth item represents gravity force, which is included in CFD coupling after setting gravity force parameter correctly.

For drag force models, different types of drag models are introduced in chapter 3 before, while in this project, Gidaspow drag force model is selected, thus the force models used in couplingProperties are: gradPForce, viscForce, GidaspowlDrag, with gravity value and transport property such as viscosity value also setting in this part.

3.2 Results and Analysis

3.2.1 Pressure Drop

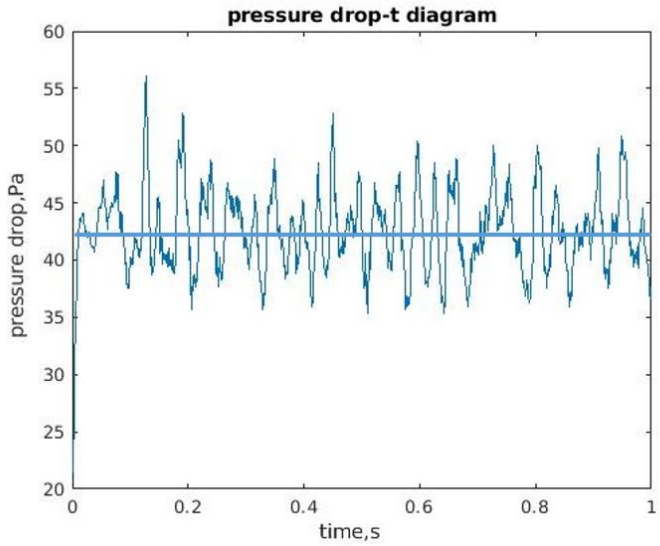

FIGURE 3.2: Pressure drop diagram versus time

The plot of pressure drop versus time are shown in figure 3.2, where the pressure drop is defined as the difference between inlet pressure and outlet pressure(which is set to be a fixed value).

From the pressure drop diagram, it could be determined that from 0s to 0.1s, the pressure drop increases immediately to around 45Pa and later suffers fluctuations. After 0.2s, the pressure drop tendency becomes to be stable of about 42Pa with $\pm 10Pa$ fluctuation. It could be seen that the maximum pressure drop in this case is about 55Pa and the minimum pressure drop is only 35Pa, with the changing ratio calculated out to be 85% to 130%.

3.2.2 Snapshots of Solid Motion

Figure 3.3 compares the snapshots at t=0.3315s between our simulation and that reported in the reference. It is clear that the bed particles motion indicated from two simulations resemble: particles are mostly tightly packed; elongated and flat bubbles are formed at the bottom of the bed and expand while travelling through the bed.

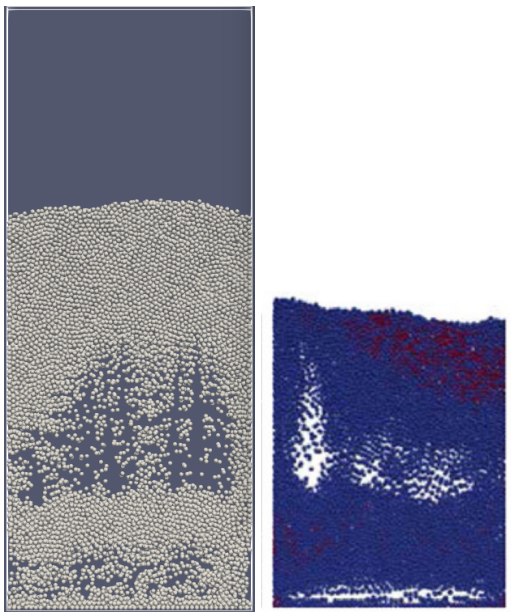

FIGURE 3.3: Contrast of simulation results(left) and paper results(right) at t=0.3315s

A series of screen snapshots of void fraction distribution at different time point (0.1s, 0.15s, 0.175s, 0.3s) are shown in figure 3.4, from which the motion tendency of particles could be observed directly:

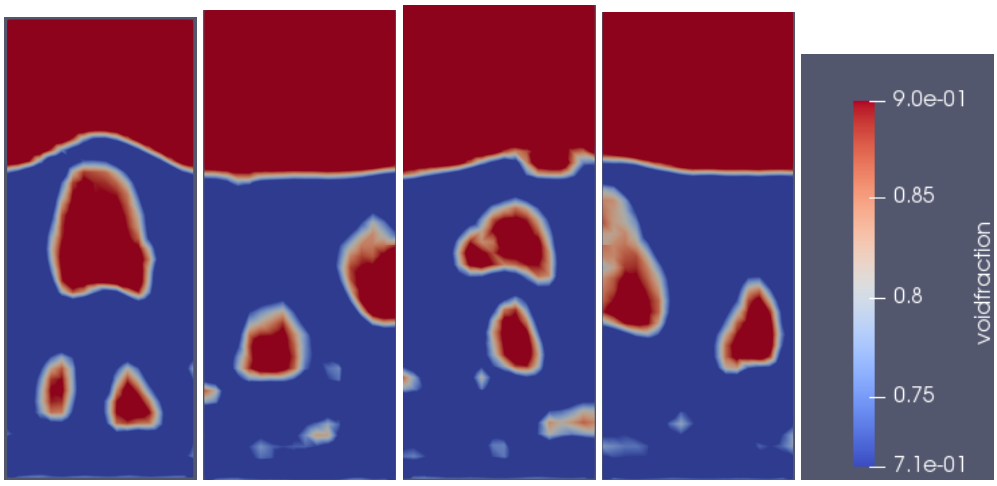

FIGURE 3.4: Snapshots of void fraction distribution at different time points

It can be seen that in this case, bubbles are formed at the very beginning and begin to rise up. There only exists a few bubbles in the whole domain, about 3

bubbles a frame, while the diameter of each bubble is relatively large, indicating that the case tends to form larger bubbles but smaller quantity.

3.2.3 Bubble Size

When analyzing, a bubble/crack is defined as a closed domain whose components have a larger than 0.8 void fraction, with the void fraction data at different time points could be read in each process folder. The bubble diameter is defined as the diameter of a sphere having the same volume of the bubble.

By the definition, bubbles of a certain time point could be detected by the mean of matlab tools(codes in appendixF)with their diameters. The main idea of analyzing these bubble data is to collect the diameters of all bubbles at each time spot in a continuous time period and calculate the probability for bubbles with different diameters. The result is shown in figure 3.5:

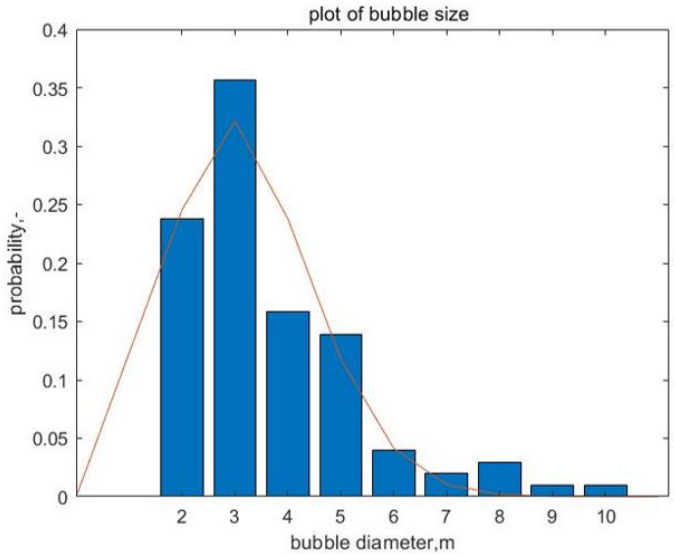

FIGURE 3.5: Plot of bubble diameters

In figure 3.5, y coordination represents the appearing frequency of different size of bubbles(which also corresponds to the probability), while these data could be fitted by Rayleigh distribution. It could be found that the amount of bubbles whose diameter is $3 \times 10^{-3} m$ appear most and the larger the diameter, the lower the probability of appearance.

3.2.4 Velocity Vector Plot

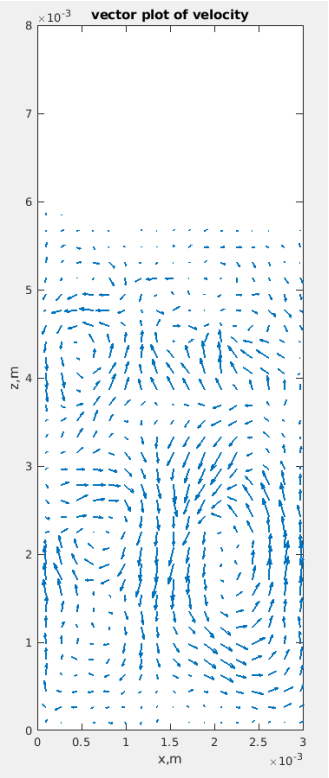

FIGURE 3.6: Vector plot of velocity

The time-average particle velocity vector plot is shown in figure 3.6. It could be seen that the there exists two symmetrical circles near the inlet, showing that the particle motion tends to rise up in the middle and than fall down close to the walls. This observation is typical characteristic of bubbling fluidized bed, where the formation of bubbles induce the circulation patterns of the solid particles.

Chapter 4

Acoustic Force Application

4.1 Case Introduction and Models Settings

In this part, the effects of cohesive force on fluidization process and acoustic force on cohesive particles are studied. To observe the effects visibly, the diameter of particles is changed to $20\mu m$(geldart A particle) and three main cases are introduced.

The first is the simple case of non-cohesive particles, whose fluidization process is typical(case 1). The second case is of cohesive particles(case 2) and the third is for sound-assisted fluidized bed for cohesive particles(case 3).

4.1.1 Re-scaled Tiny Particles

Firstly, as a correspond to the change of particle diameter, other geometrical parameters and physical properties for simulations in this chapter are presented in Table 4.1.

For the determination of time step in Hertzian contact model, the collision time is defined as

$$t_{coll} = 2.943\left(\frac{5\sqrt{2}\pi\rho(1-\nu^2)}{4Y}\right)^{\frac{2}{5}}\frac{R}{v_0^{\frac{1}{5}}} \tag{4.1}$$

while $t_{DEM} = \frac{t_{coll}}{50}$ is used in this case.

Inlet velocity is determined by the balance equation between gravity and drag force, since KochHill drag model is selected in this section, the minimum fluidization velocity is calculated as 0.0025m/s, thus the inlet velocity is chosen to be $v_i = 2v_{mf} = 0.005m/s$.

The setting details are shown in table 4.1.

4.1.2 Cohesive Particles

The second case is the case for cohesive particles, while the cohesive force is implemented according to the equation (2.12) and (2.13). There are two parameters, Ha and minimum surface distance between particles s_{min}, which are also shown in table 4.1.

Two other cohesive models are also carried out in Appendix C, of which the result comes out that the effect of original van der Waals model is the most obvious and is chosen in this chapter.

TABLE 4.1: Parameters of the case simulation of tiny particles

parameter	value	unit
Geometry(length x, width y, height z)	$1.08 \times 0.06 \times 2.52$	mm
Cell size($\delta x, \delta y, \delta z$)	$0.06 \times 0.06 \times 0.06$	mm
Particle number	10000	-
Particle diameter d_p	20	μm
Inlet velocity u_i	0.005	m/s
Gas density ρ_g	1.205	kg/m^3
Gas dynamic viscosity μ_g	1.81×10^{-5}	$Pa \cdot s$
Gravity g	9.81	m/s^2
Particle density ρ_p	2250	kg/m^3
Young's modulus Y	10^8	Pa
Hamaker constant A	2.1×10^{-21}	J
Poisson's ratio ν	0.22	-
Restitution coefficient e	0.94	-
Sliding friction coefficient μ_s	0.18	-
Minimum separation distance s_{min}	1	nm
Simulation time of CFD t	5×10^{-6}	s
Simulation time of DEM t_{DEM}	5×10^{-8}	s
coupling interval n	100	-

4.1.3 Cohesive Particles with Sound-assisted Field

Before adding, the acoustic force needs to be implemented into cfdem force library with its properties to be set in couplingProperties file in constant folder, which is writted as: velFieldName "U"; densityFieldName "rho"; voidfractionFieldName "voidfraction". The other settings remain the same with cohesive case without acoustic force, thus the effects of the extience of acoustic force could be discussed by contrasting these two cases.

The existence of acoustic field will cast a additional force on particles, for which the equation is given by equation (2.20) as mentioned in the chapter 2, which is quite similar to the expression of drag force, thus the implement of acoustic is easy by modifying a drag force model to just calculating β_{gs} by replacing u_g by u_{ac} in the equation of drag force, while in this case, KochHill drag model is used.

In this section, acoustic wave with a spl of 140dB and frequency of 100Hz is considered, while acoustic wave applications with other different parameters are carried out later in section 4.3.

4.2 Results

4.2.1 Pressure Drop

The first to discuss is the time when steady state is approached, thus the pressure drop versus time plot is needed, which is shown in figure 4.1.

Figure 4.1 shows the pressure drop of case 1(red line), case 2(blue line) and case 3(green line). From figure 4.1, it could be found that for all of these three cases, the pressure tends to increase immediately at the very beginning, and then decrease into a relatively steady value with some fluctuations. There also exists some obvious differences. For case 2, the stable value of pressure drop is only about 10 Pa, which is lower than the other two cases (about 15 Pa). For case 3, although the stable value is

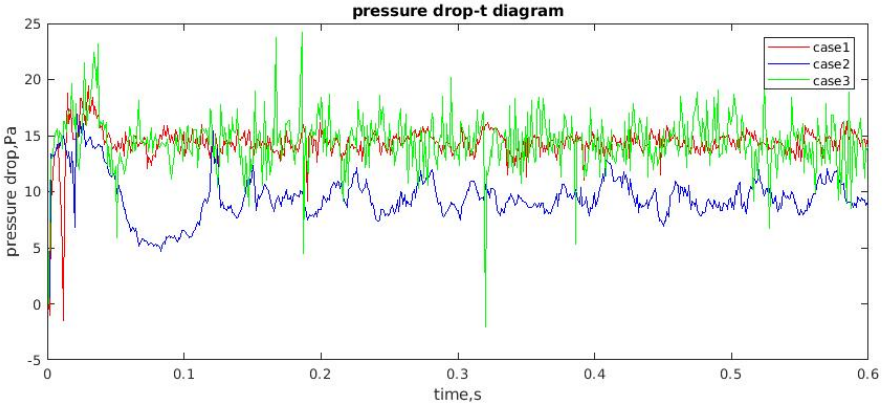

FIGURE 4.1: Pressure drop diagram versus time, case 1(benchmark), case 2(with vdw force), case 3(with vdw force and acoustic force)

almost the same as case 1, it suffers more fluctuations with an amplitude even up to $\pm 10Pa$. The time when the steady state is approached also differs: case 2 uses more time(about 0.15s) to reach a steady state, while case 1 and case 3 use only 0.05s.

An assumption to this phenomenon is that when compared with case 1, particles of case 2 suffer a strong cohesive force, which makes them tend to agglomerate into larger particles. When agglomerates are formed in the area, the movement of air molecules slows down, and thus the pressure drop level of case 2 with cohesive force is lower than case1. When an acoustic force is added in case 3, the agglomerations may be broken and thus speed up the movement of air molecules, which corresponds to a higher pressure drop level. Since the acoustic wave is a kind of sine wave, the probability of uncertainty would increase and thus the fluctuation amplitude also increases.

4.2.2 Instantaneous Snapshots

The snapshots at different times for all cases are shown in figure 4.2. Gas blow up from the bottom and carries particles along, while bubbles are formed during this process and break down when raise to the highest point.

Figure 4.2 shows snapshots of case 1(benchmark case), case 2(with vdw force), case 3(with vdw force and acoustic force) at time point of 0.05s, 0.1s, 0.3s. 0.33s and 0.36s. The reason for choosing these time points is that 0.05s and 0.1s correspond to the initial state, while after 0.3s particles must approach the steady state. In order to observe particle or bubble motions, a smaller time step is need and 0.03s as a choice.

In figure 4.2, when comparing case 1 with case 2, it could be found that the number of bubbles of case 1 is much more than case 2, while the slugging phenomenon in case 2 is obvious and the size of particle agglomerates(dense solid region) is much larger. When acoustic force is added, the area of dense solid region becomes smaller, which indicates that the agglomeration phenomenon is weakened.

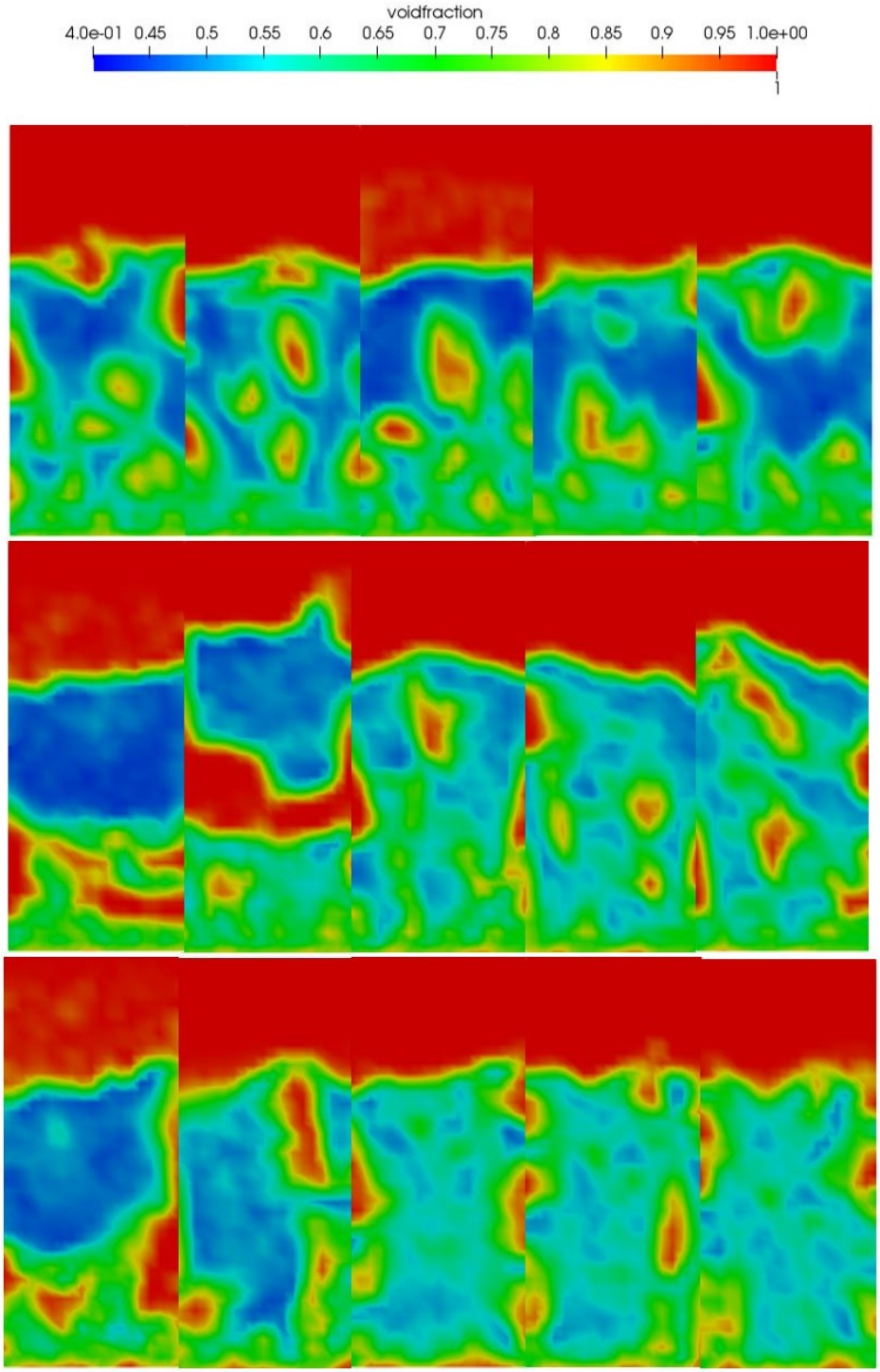

FIGURE 4.2: Snapshots at different time points0.05s,0.1s,0.3s,0.33s,0.36s of case 1,2,3

4.2.3 Particle Cloud Result

To observe the behavior of particles, snapshot of particles velocity is recorded. Figure 4.3 shows that for cohesive particles, agglomerations are formed with a low velocity closing to 0, which means that particle agglomerates move slowly and contact tightly. When acoustic force is added in the system, void area increases between

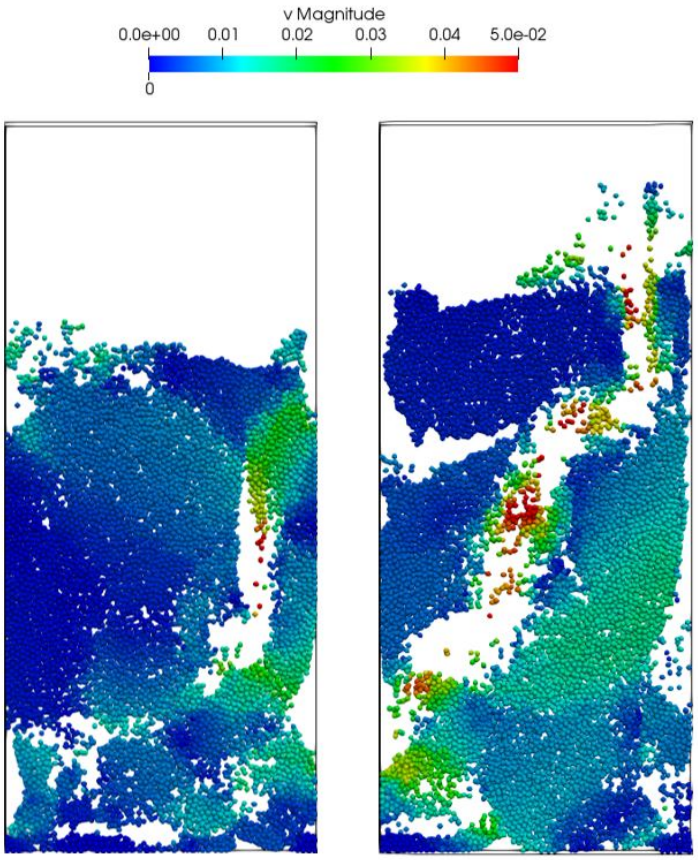

FIGURE 4.3: Snapshots of particles velocity at t=0.33s of cohesive case(left) and acoustic case(right)

particle agglomerates and the moving velocity of agglomerations becomes larger comparing to the case without acoustic force with the disappearance of channeling and slugging in the bed.

4.2.4 Bubble Size

The probability plot of different size of bubbles of all cases are shown in figure 4.4.

Figure 4.4 shows that the number of bubbles whose size is 40 times of particles in case 1 is the highest, which is up to 0.7, indicating that bubbles of case 1 are relatively small but of a large quantity. When cohesion model is considered, the probability of small bubble decreases and probability of large bubble increases, which corresponds to the assumption that particles tend to form agglomerations in cohesion case and thus the probability of small bubble decreases; the slugging phenomenon also explains the increase of large bubbles. In case 3, acoustic force is added, the quantities of total bubbles increase.

4.2.5 Agglomeration Size

In order to describe the degree of agglomeration phenomenon, a useful way is to detect the sizes of each agglomeration and draw a pdf plot to see the probability of different sizes of agglomerations. The main idea to detect sizes of agglomeration is that, firstly find particle pairs which are contact with others, for example, if the

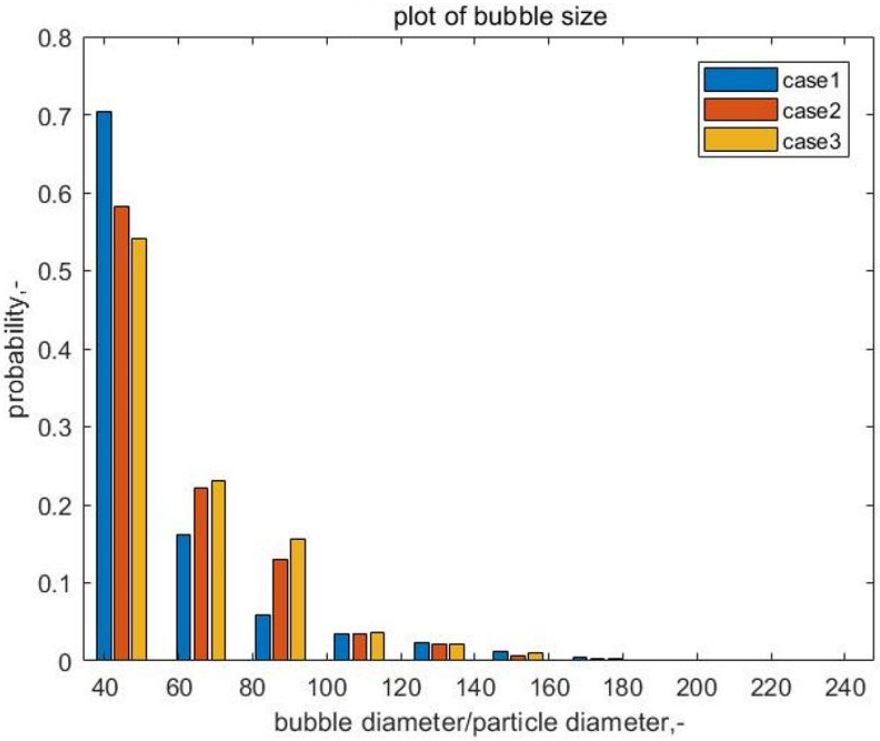

FIGURE 4.4: Plot of bubble diameters of case 1,2,3

distance between two particles is smaller than the diameter of a single particle, these two particles are regarded to contact with each other. Second step is to detecting particle pairs who have one same particle id and record the data. An additional step is to find out the pair data at next time step and compare it with previous one to figure out whether pairs recorded are in collision or agglomeration. Using matlab code, the data of particle pairs could be recorded and also pdf plot of agglomeration size, which is shown as fig 4.5 and 4.6.

Figure 4.5 shows the probability density distribution(pdf) plot of particle agglomerates with its typical agglomeration shape. The red line shows the fitting line for the data, which corresponds to an exponential distribution, with the expression written as $p = 0.5317e^{-0.1915x}$. Similarly, the data and fitting line with the expression $p = 0.5547e^{-0.2103x}$ of acoustic case are shown in figure 4.6 with a typical agglomeration size.

In figure 4.5, it could be easily seen that there exists particle agglomerates consisting of large quantities of particles, of which the maximum number of particles is up to 70 particles, while in figure 4.6, the largest particle agglomerates for the acoustic case only consists of 40 particles. When comparing figure 4.5 and 4.6, it is found that the probability of smaller agglomerates increases when acoustic field is applied and the number of large agglomerates decreases a lot, which indicates that the probability of agglomerations does decrease with the assistance of sound wave.

A typical value of agglomeration size could be estimated by the expression of the fitting lines, while the size calculated out for cohesive case is $s_{co} = \frac{0.5317}{0.1915^2} = 14.49$ and the typical value for acoustic case is $s_{ac} = \frac{0.5547}{0.2103^2} = 12.54$.

4.2.6 Velocity

The vector plots of velocity for all cases are shown in figure 4.7.

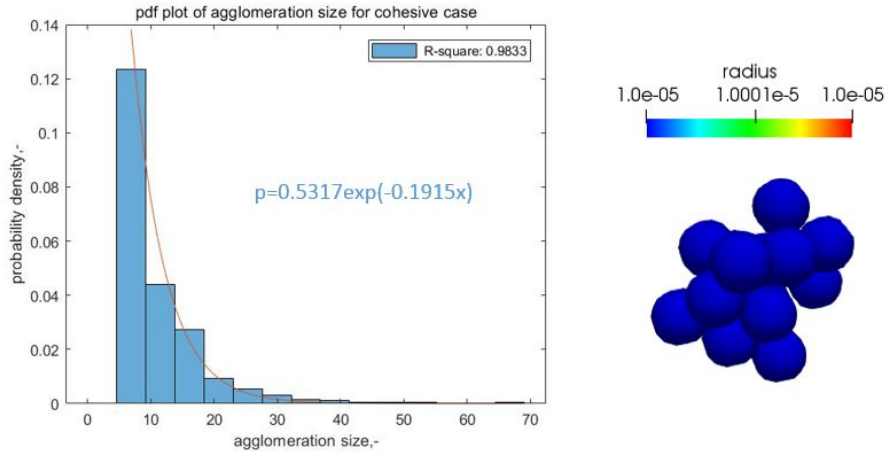

FIGURE 4.5: Pdf plot of agglomeration size of case 2(left) with a typical shape(right)

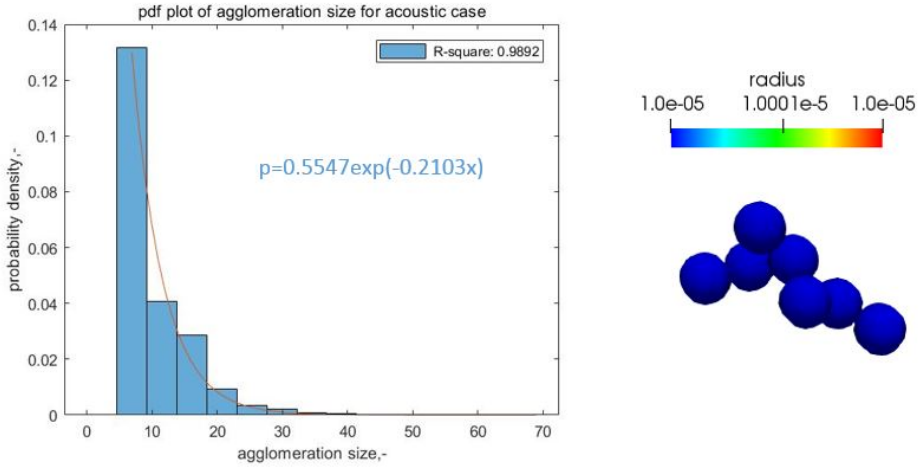

FIGURE 4.6: Pdf plot of agglomeration size of case 3

In figure 4.7, it could be seen that there exists two symmetric circles in the velocity vector plot for non-cohesion case, which indicates the existence of vortexes. The size of the circle is about 0.5mm diameter of case 1. When cohesive force is added in case 2, circles decompose and another big circle is generated at the top of the bed with a diameter of 1mm. For case 3, with the assistance of acoustic field, two symmetric ellipses appear with the eccentricity of about 0.7. Comparing case 1, 2 and 3, it could be found that when cohesive force is added, the shape of vortex circles would be changed while at the bottom of the bed, the circles shape remains even smaller than the original case; when acoustic force is added on the cohesive case, the large circle at the top tends to break down and the shape of circles at the bottom becomes longer, even more like an ellipse. This phenomenon also corresponds to the fact that in a cohesive case, particles tends to form agglomerations and the motions of particles become slower, while with the assistance of a sound field, the agglomerations would be partly broken.

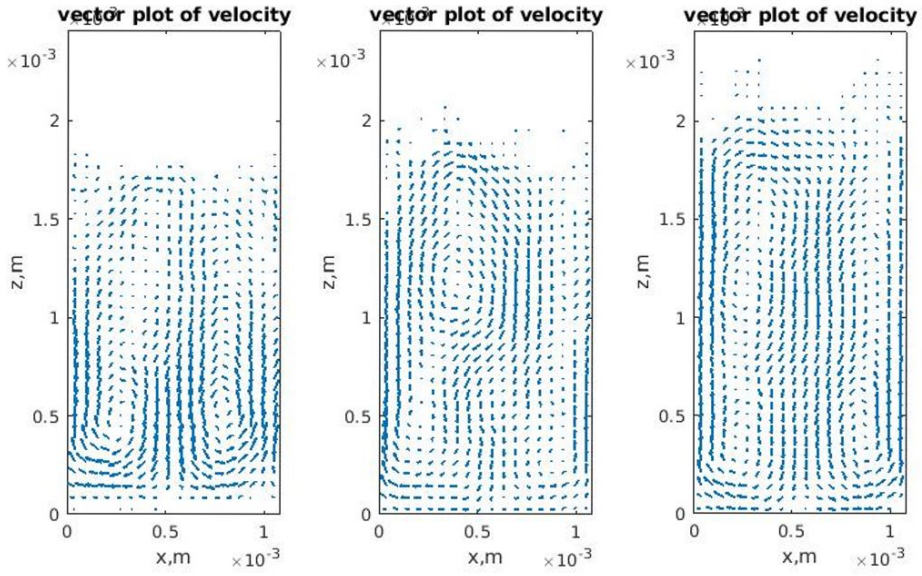

FIGURE 4.7: Vector plot of case 1(left),2(middle),3(right)]

4.3 Effects of Acoustic Frequency

As discussed before, the main parameter of an acoustic wave is its frequency and sound pressure level value, thus the effects of applying acoustic waves with different frequency is necessary to be studied in this section. The main idea is to simulate a simple case with acoustic waves of different frequency and spl and compare their agglomeration properties. In this project, frequency of 20Hz, 50Hz, 80Hz, 100Hz and 120Hz and spl of 100dB, 120dB and 140dB is selected.

4.3.1 Effects on Agglomeration Size

Figure 4.8 shows the fitting lines of pdf plots of agglomeration sizes for cases with different frequency at the sound pressure level of 100dB(with the red line corresponds to the case of 20Hz, blue line corresponds to the case of 50Hz, green line corresponds to the case of 80Hz, cyan line corresponds to the case of 100Hz and magenta line corresponds to the case of 120Hz). In the zoom-in plot, the differences between these cases are easily to be seen. It is shown that when applying an acoustic field with a frequency of 20-80Hz, the fitting lines become lower with the increase of frequency, which indicates that the agglomerates are becoming smaller, However, when frequency increases from 80Hz to 100Hz, the fitting lines become higher, which means that the agglomerate sizes become larger again. It could be summarized that with a frequency of 80Hz, the agglomerations are the smallest, which also reflects that the effects are the most strong in this case.

However, the difference between different cases is not obvious, which indicates the fact that the effects acoustic force cast on cohesive particles are not severe.

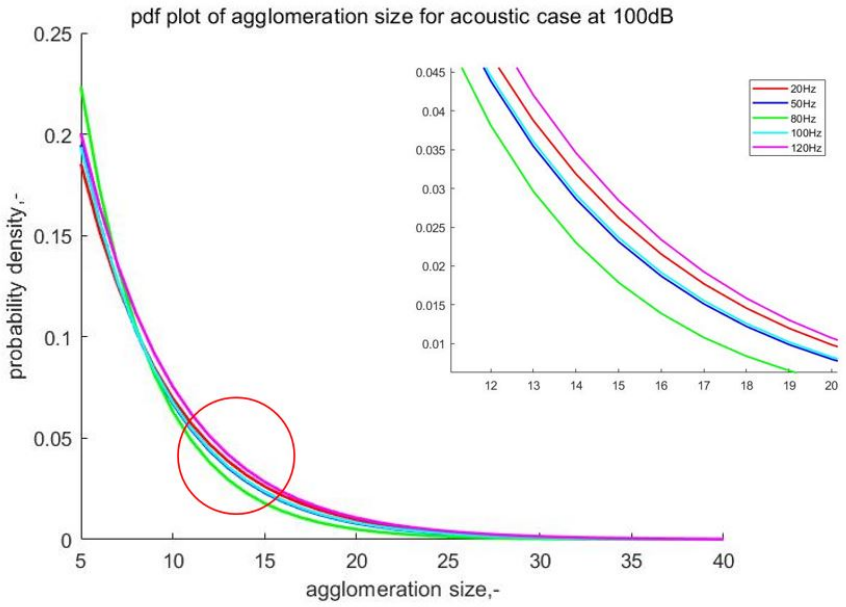

FIGURE 4.8: Pdf plot of agglomeration size at spl of 60dB

4.4 Effects of Sound Pressure Level

Similarly, figure 4.9 shows the fitting lines of pdf plots of agglomeration sizes for cases with different spl at the frequency 100Hz. It could be found that with the increase of spl value, the fitting lines become lower, which illustrates that the particle agglomerates tend to be smaller with the increase of spl from 100dB to 140dB, corresponding to a conclusion that the larger spl value, the stronger the acoustic force.

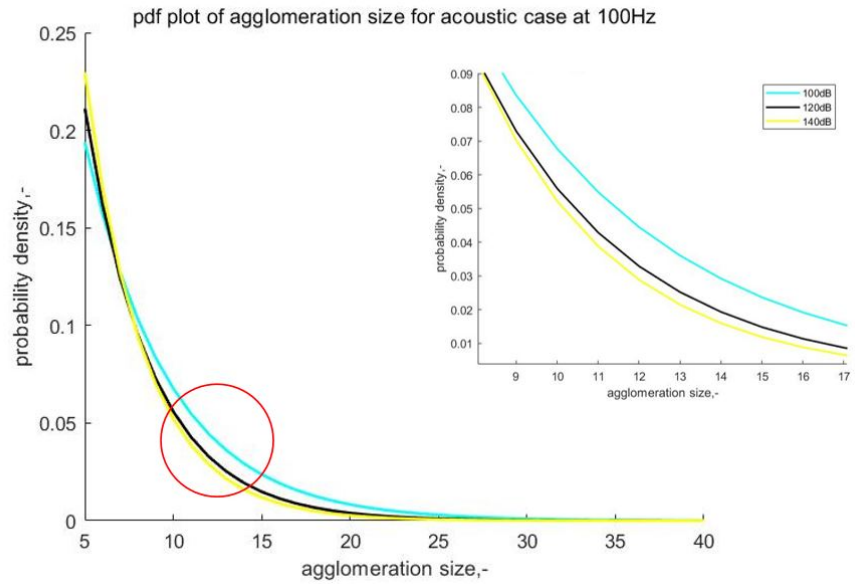

FIGURE 4.9: Pdf plot of agglomeration size at fre of 100Hz

Chapter 5

Acoustic Application on Large particles

5.1 Introduction and Model Settings

For the reason that numerical simulations for fine particles are really difficult to be treated by DEM since the existence of volume limit, which also affects resolutions for the results, a larger size of particles of diameter 1.0 mm is considered in this part(group B particles), while this also speeds up the simulation to reach the fluidization condition. The parameters of the case are shown in table 5.1.

TABLE 5.1: Parameters of the case simulation of larger particles

parameter	value	unit
Geometry(length x, width y, height z)	$54 \times 3 \times 150$	mm
Cell size($\delta x, \delta y, \delta z$)	$3 \times 3 \times 3$	mm
Particle number	10000	-
DEM time step t	5×10^{-7}	s
CFD time step t	5×10^{-5}	s
Particle diameter d_p	1	mm
Particle density ρ_p	2250	kg/m^3
Hamaker constant of particle A	1.5×10^{-18}	J
Minimum separation distance s_{min}	1	nm
Acoustic field frequency f_{ac}	100	Hz
Sound pressure level spl	120	dB
Gas density ρ_g	1.205	kg/cm^3
Gas dynamic viscosity μ_g	1.81×10^{-5}	$Pa \cdot s$
Inlet velocity u_i	1	m/s

In this chapter, three main cases are taken into consideration: case 1 is the no-cohesion case, case 2 the case for particles with van der waals force and case 3 adds an acoustic force on the base of case 2, of which the frequency and spl value are also shown in table 5.1.

However, for large particles, the effects of cohesive force(mainly van der waals force as mentioned before) and acoustic force are relatively insignificant. In order to mimic the cohesive effect for fine particles, Tatemoto et al. [6] proposed an equation given by:

$$f_{vd,1mm} = (\frac{d_{1mm}}{d_{20\mu m}})^3 f_{vd,20\mu m} = K_{vd} f_{vd,20\mu m} \tag{5.1}$$

The modification of acoustic force is similar to van der waals force:

$$f_{ac,1mm} = (\frac{d_{1mm}}{d_{20\mu m}})^3 f_{ac,20\mu m} = K_{ac} f_{ac,20\mu m} \tag{5.2}$$

In software scripts of previous case, van der waals force is given by:

$$F_{vdw}(A,s) = \frac{A2r_i r_j(r_i+r_j+s)}{3s^2(2r_i+2r_j+s)^2}[\frac{s(2r_i+2r_j+s)}{(r_i+r_j+s)^2-(r_i-r_j)^2} - 1]^2 \tag{5.3}$$

When the diameter of particles is 1mm, the order difference between particle diameters(order of 1e-3) and particle distance(order of 1e-10) is really large and thus the equation of van der waals could be simplied as:

$$F_{vdw}(A,s) = \frac{A2r_i r_j(r_i+r_j)}{3s^2(2r_i+2r_j)^2}[\frac{s(2r_i+2r_j)}{(r_i+r_j)^2-(r_i-r_j)^2} - 1]^2 = \frac{A2r^2(2r)}{3s^2(4r)^2}[\frac{4sr}{4r^2} - 1]^2 = \frac{Ar}{12s^2} \tag{5.4}$$

Thus the van der waals for 1mm particles are given by:

$$f_{vd,1mm} = (\frac{d_{1mm}}{d_{20\mu m}})^3 f_{vd,20\mu m} = (\frac{d_{1mm}}{d_{20\mu m}})^3 \frac{Ad_{20\mu m}}{24s^2} = (\frac{d_{1mm}}{d_{20\mu m}})^3 \frac{d_{20\mu m}}{d_{1mm}} \frac{Ad_{1mm}}{24s^2} = 2500\frac{Ad_{1mm}}{24s^2} \tag{5.5}$$

Similar, the equation for acoustic force applied on 1mm particles is given by:

$$f_{ac,1mm} = (\frac{d_{1mm}}{d_{20\mu m}})^3 f_{d,20\mu m}(\frac{d_{1mm}}{d_{20\mu m}})^3 \frac{\beta_{gs} V_{p20\mu m}}{1-\varepsilon_g}(u_{ac}-v_p) = \frac{\beta_{gs} V_{p1mm}}{1-\varepsilon_g}(u_{ac}-v_p) \tag{5.6}$$

All equations proposed above is on the assumption that the granular Bond number(Bo, defined as the ratio of cohesive force to particle weight) remains the same when particle size is changed from $20\mu m$ to $1mm$, another method is to use a scale factor(defined as the ratio of the cohesive force to the buoyant weight of a single particle) proposed by Wang et al. [25, 36]. For the group B particle in this chapter, the scale factor of 3 and is over 40 for cohesive numbers, thus the equation of amplified van der waals force is given by:

$$f_{vd,1mm} = \frac{3}{40}(\frac{d_{1mm}}{d_{20\mu m}})^3 \frac{d_{20\mu m}}{d_{1mm}} \frac{Ad_{1mm}}{24s^2} \tag{5.7}$$

After modification, the effects of cohesive force and acoustic force could be estimated in this part, with other parameters shown in table 5.1.

5.2 Results

5.2.1 Pressure Drop and Bed Height

The first to observe is still the pressure drop tendency. Since the fluidization for large particles are more difficult to reach a steady state, the end time of computing is set to be much longer than the tiny cases, which is about 5.0s.

However, the result of pressure drop plots for case 3 suffers a lot of fluctuations and the average value of pressure drop are almost the same, while the pressure drop tendency for case 2 and case 1 are much more stable when compared to the other line. In order to analyze the steady state in a visible way, the bed height plot is instead and shown in figure 5.1.

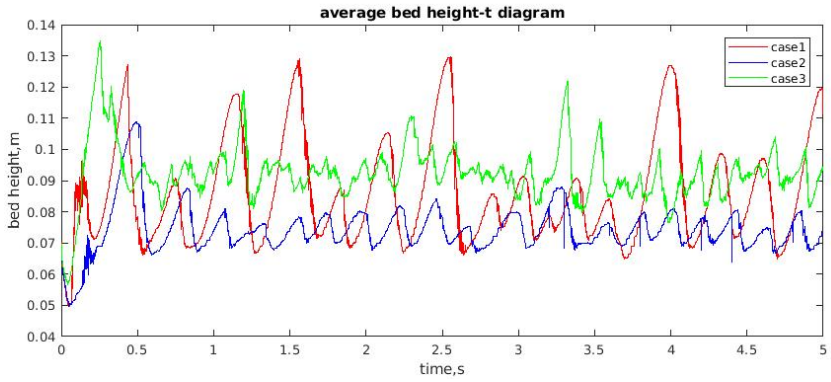

FIGURE 5.1: Bed height diagram versus time of case 1,2,3

In figure 5.1, the fluctuations of all cases become visible to be observed. In the first 0.3s, the average bed height of case 3 increases rapidly, while the highest value of case 3 is 0.135m and the highest value of case 1 is 0.125m, 0.01m lower than case3. Meanwhile, the average bed height of case 1 and 2 increase slower in 0.5s and only reach a highest value of 0.11m. The average bed height of cohesion case is the lowest, which is only about 0.075m, half the whole bed height. While average of original case 1 and acoustic case 3 is about 0.095m, 0.02m higher than the average bed height of cohesive case.

Meanwhile, the fluctuation amplitude of cases also differs from each other. The fluctuation amplitude of case 2 is the lowest, only about $\pm 0.01m$, while the fluctuation amplitude of case 1 is the highest, even up to 0.06m. Also, the fluctuation of case 3 is the most unstable one, with the largest fluctuation amplitude up to 0.02m and the smallest 0.005m.

These results could be explained by an assumption that without a cohesive force, particles perform the property of fluidization well while for particles with cohesive force, they tend to form agglomerates and the distribution of particles would become tighter than those particles without a cohesive force. When acoustic force is applied, the agglomerates would be broken and the motion of particles become more active, thus the higher average bed height would be reached. The result in this section of large particles also corresponds to the result in chapter 4.

5.2.2 Screen Snapshots

The screen snapshots of three cases are shown in figure 5.2.

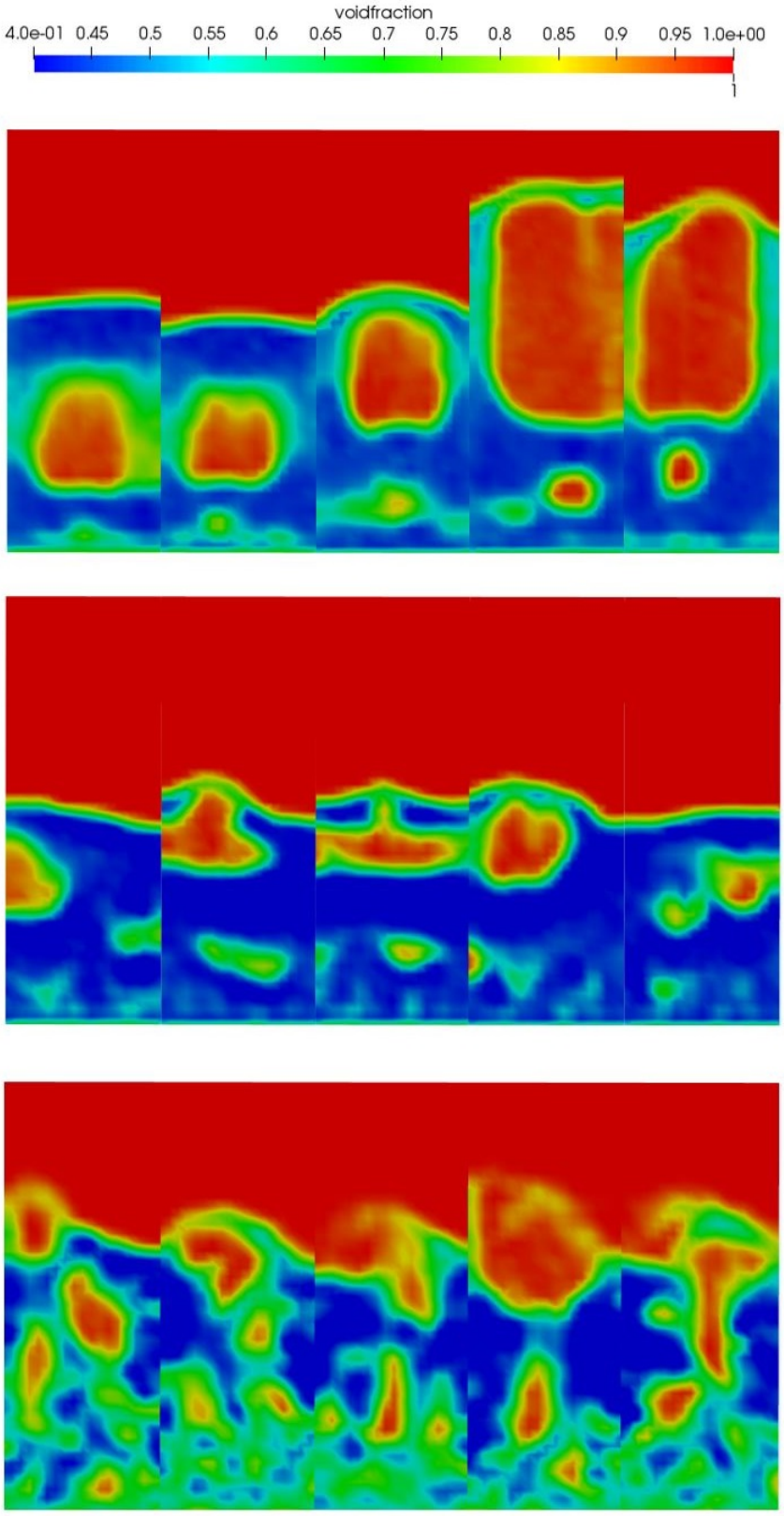

FIGURE 5.2: Screen snapshots of case 1,2,3 at time 1.0s, 2.0s, 3.0s, 4.0s, 5.0s

The first row of figure 5.2 shows the fluidization for non-cohesion particles. It

is shown that bubbles are generated at the bottom and then raise up to the top until it breaks, which is much like a classic fluidized bed's behavior. Figure 5.3 also illustrates that the area and depth of dense solid region increases a lot when comparing case 1 and case 2, which indicates that agglomerates of particles are formed and a slugging mode also exists in case 2. In case 3, when acoustic force is added, the area and depth of densolid region decrease a lot and the number of small bubbles increases with the disappearance of slugging modes, which also illustrates the fact that with the assistance of a sound field, the agglomerates of particles do break down.

When compared to the cases for fine particles in chapter 4, the results show that the bubbles become much more and the fluidization process of large particles are easier to approach.

5.2.3 Particle Cloud Result

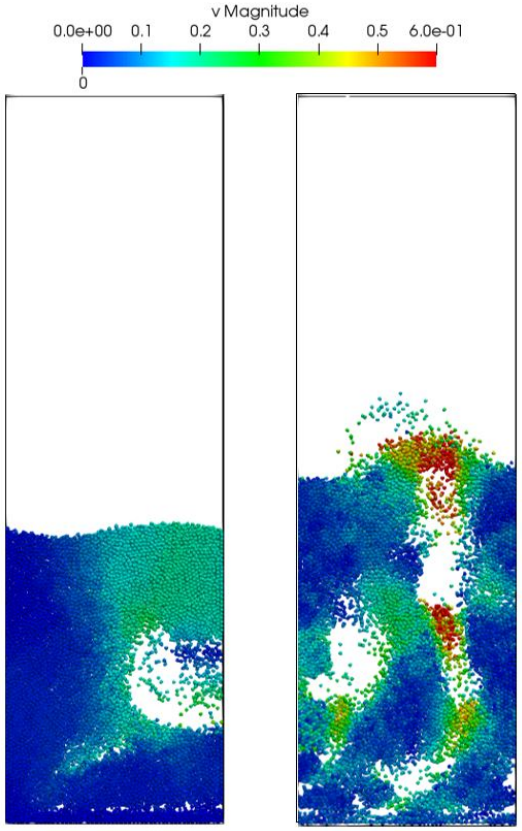

FIGURE 5.3: Snapshots of particles velocity at t=0.33s of cohesive case(left) and acoustic case(right)

The snapshots of particles for case 2(with vdW force) and case 3(with vdW force and acoustic force) are shown in figure 5.3, from which the effects of acoustic force on cohesive particle behaviors could be easily found. The left one shows that in the cohesive case, particle agglomerates are formed with a slugging mode. The velocity of most particle is relatively low, closing to 0, while larger velocity only appears at the boundary of bubbles. In the right figure of 5.4, it could be easily seen that the agglomerates of particles become smaller with a larger velocity of particles when acoustic force is applied. When comparing these two cases, it could be found that void area increases a lot with disappearing of slugging area, which indicates that particle agglomerates are partly broken by acoustic waves.

5.2.4 Bubble Size

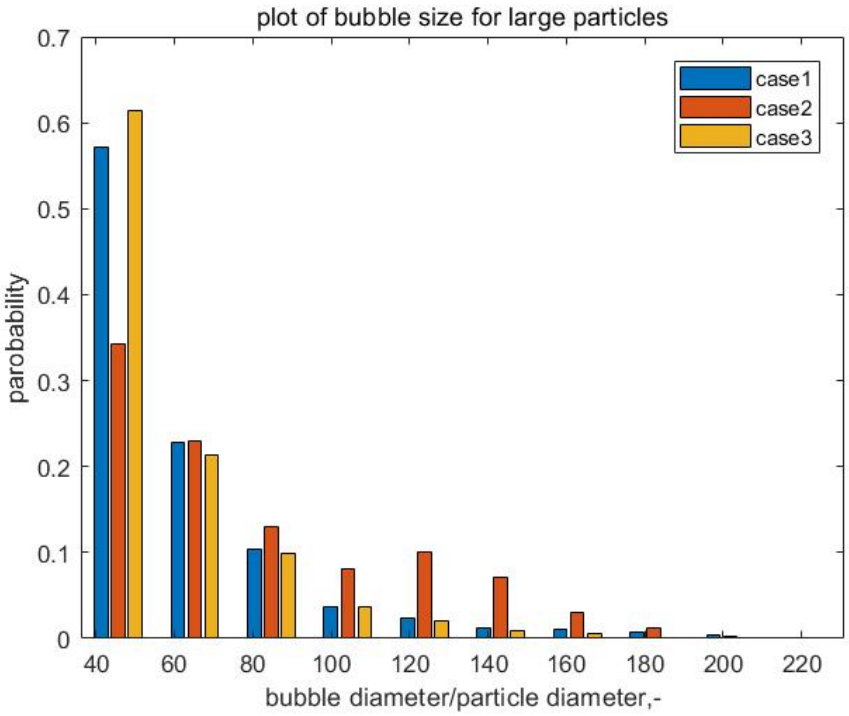

FIGURE 5.4: Plot of bubble size of case 1,2,3

The pdf plot of bubble size is shown in figure 5.4. It could be found that for cohesive particles, the probability of large bubbles is the highest, which corresponds to the extience of a slugging mode; probability of small bubbles is much lower than the original case, while when acoustic field is added, the probability of small bubbles increases again, which also corresponds to the result and analysis in screen snapshots section.

5.2.5 Agglomeration Size

In figure 5.5 and 5.6, the agglomeration pdf plots for case 2,3 with its typical agglomerate size are illustrated and the differences are obvious. It could be found that for larger particles, the agglomeration phenomenon is not notable. However, when cohesive force model is added, the agglomeration number of particles increases a lot and become similar to the results obtained in chapter 4. When sound field is added, the number of agglomerations decreases again and the largest agglomeration is only about 15 pairs of particles.

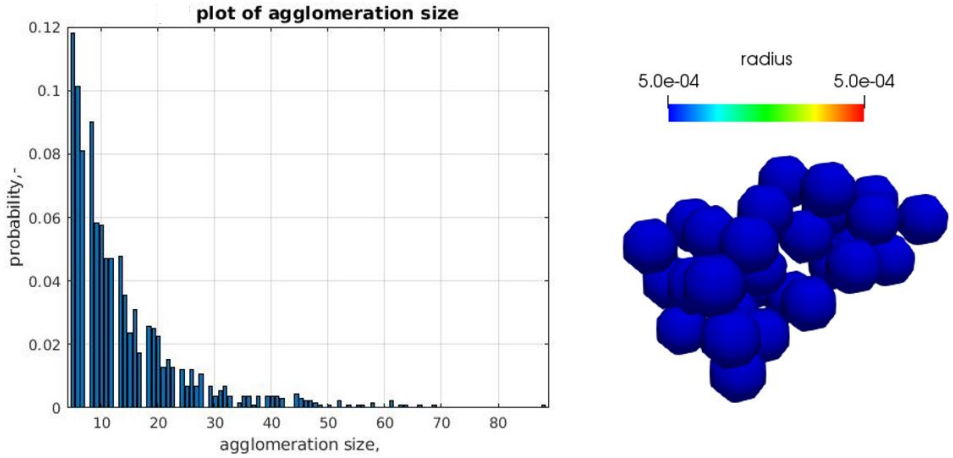

FIGURE 5.5: Pdf plot of agglomeration size of case 2(left) with its typical shape(right)

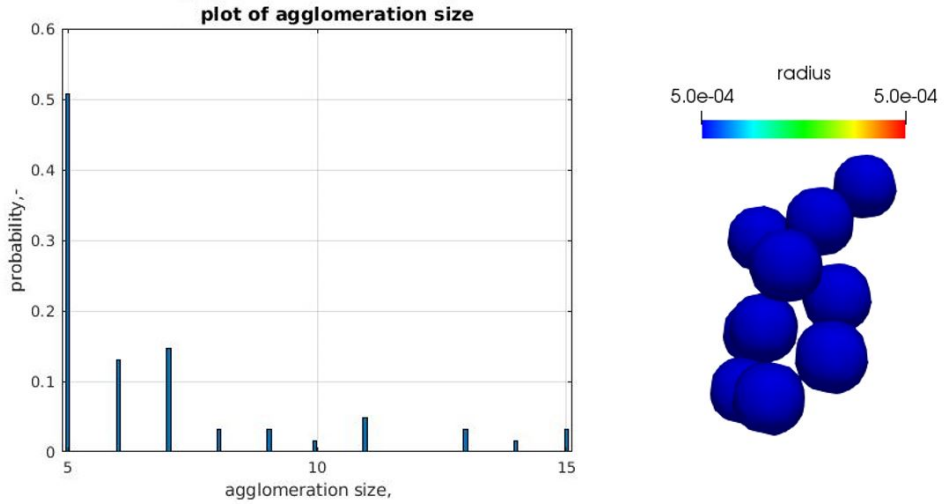

FIGURE 5.6: Pdf plot of agglomeration size of case 3(left) with its typical shape(right)

5.2.6 Vector Plot of Velocity

Figure 5.7 shows the velocity vector plot of three cases. In the first diagram, it could be found that there exists two vortex circles near the top of the bed, with the length relatively long; When cohesive force is added, the original vortexes disappear and another big vortex appears at the center of the bed; With the assistance of acoustic field, the large vortex at the center disappears and two long vortex circles appear again, but not notable. Those phenomena could be explained by the reason that when cohesive force plays an important role in case 2, particles tends to move together as a whole agglomerate and the symmetric vortex circles are easy to be broken, while with the assistance of sound field, the appearance probability of large agglomerations decreases and begins to break into small ones and thus the motion of particles would become similar to those particles in case 1, but not really the same.

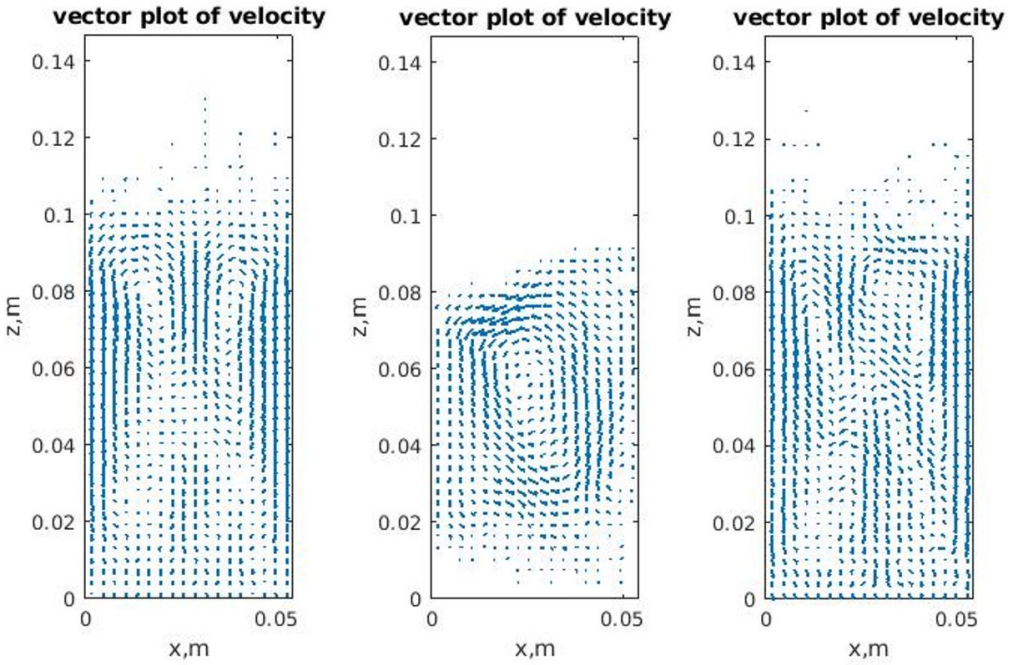

FIGURE 5.7: Vector plot of velocity of case 1(left),2(middle),3(right)

Chapter 6

Conclusion and Recommendation

6.1 Conclusion

In this project, the agglomeration phenomenon of cohesive particles in a pseudo-2D fluidized bed(with the size $1.08mm \times 0.06mm \times 2.52mm$ and $54mm \times 3mm \times 180mm$) is studied. The application of acoustic field is investigated on its influence on the breakup of particle agglomeration.

Firstly fine particles with diameter of 20 micron-meters are considered. Attempts have been made to test out different cohesive force model reported in literature. The original van der Waals model was in the end chosen and implemented for the cohesive force on particles in the simulations reported in previous chapters. Additionally, it is found that care has to be taken on the value of young's modulus. Overall, we compare simulations of benchmark with case with van der Waals force and cases with application of acoustic forces. The results shows that the application of acoustic forces can to some extent break the agglomerates of fine particles, depending on the choice of sound frequency and sound pressure level.

The simulations using fine particles (20 μm) show unsatisfying stability due to the limitation of numerical schemes of the code. Therefore, larger particles(1 mm) are then used to mimic the fine cohesive particles' behavior. To this end, the van der Waals force and the acoustic force are scaled according to empirical correlations. The results confirm the observation from simulations of fine particles. Moreover, the effect of acoustic field is found more stable and stronger, leading to much smaller and less agglomerates and more homogeneous fluidized bed.

6.2 Recommendation

The phenomenon of agglomeration and parts of effects cast by the assistance of acoustic field are already studied in this project, however, the effect is only studied at certain cases: all sound pressure level data are based on 100dB and frequency data based on 100Hz. Firstly, it would be more reliable to get data with more different parameters to see the influences of acoustic field overall.

Secondly, due to the limitation of numerical simulation on fine particles, the particle is changed into a larger scale from $20\mu m$ to $1mm$ with the amplification of van der Waals force and acoustic force correspondingly, however, the simulation is only based on an assumption, whether the result is correct needs to be proved by experiments. Also, the chosen of Hamaker constant number needs to be checked, for the reason that in the simulation of particles with a diameter of $20\mu m$ the Hamaker constant number remains the same with the validation case, while the scale factor of group A particle and group C particle differs.

Thirdly, the results show that the fluidization behaviors of cohesive particles are enhanced in the case without a temperature change, while in the application

of micro-fluidized beds, the change of temperature also needs to be considered since there may exist some heat exchange or reactions in a fluidized bed.

Appendix A

Installation Instruction

A.1 Software Installation

The general installation tutorial of CFDEM could be found on the official website of CFDEM: www.cfdem.com/media/CFDEM/docu/CFDEMcoupling_Manual.html#id2.

A.1.1 Software Download

On a linux operating system, the download is quite convenient for users to get the sources using Git, which means that installing git should be the first thing to

```
sudo apt-get install git-core
```

If the system returns the fact that it is unable to update apt, there are two ways to solve the problem:(1)update the version of ubuntu operation system;(2)replace the contents of /etc/apt/sources.list in the source file with an old released version.

From github, one can download CFDEM and LIGGGHTS package, for which the code is shown below:

```
cd $HOME
mkdir CFDEM
cd CFDEM
git clone git://github.com/CFDEMproject/CFDEMcoupling-PUBLIC.git
cd $HOME
mkdir LIGGGHTS
cd LIGGGHTS
git clone git://github.com/CFDEMproject/LIGGGHTS-PUBLIC.git
git clone git://github.com/CFDEMproject/LPP.git lpp
```

In order to download the correct version of OpenFOAM, firstly the suitable version should be determined, which could be found in the fold: CFDEM/CFDEMcoupling-PUBLIC-/src/lagrangian/cfdemPartilce/cfdTools/versionInfo.H/, where in the line: word OFversion="<OF-Release>-commit-<commitHashtag>";

The code of downloading of the correct version of OpenFOAM is shown below:

```
cd $HOME
mkdir OpenFOAM
```

```
cd OpenFOAM
git clone git://github.com/OpenFOAM/OpenFOAM-<OF-Release>.git
git clone git://github.com/OpenFOAM/ThirdParty-<OF-Release>.git
cd OpenFOAM-<OF-Release>
git checkout <commitHashtag>
```

A.1.2 setup prerequisites

Prerequisites for CFDEM project are shown as below:

```
sudo apt-get install build-essential flex bison
cmake zlib1g-dev libboost
-system-dev libboost-thread-dev
libopenmpi-dev openmpi-bin gnuplot
libreadline-dev libncurses-dev libxt-dev
libscotch-dev libptscotch-dev
sudo apt-get install libvtk6-dev
sudo apt-get install python-numpy
```

A.1.3 Installation and Compilation for OpenFOAM

To install OpenFOAM, firstly open the bashrc file by typing the code:

```
gedit /.bashrc
```

and then add two lines in the end, which is shown as below, where $< NofProcs >$ is the integer number set and $< OF - Release >$ the version name of the suitable OpenFOAM.

```
export WM_NCOMPPROCS=<NofProcs>
source $HOME/OpenFOAM/OpenFOAM-<OF-Release>/etc/bashrc
```

The next step is to set environment variables and path. Firstly, tag the CFDEM coupling folder with the OpenFOAM version number by:

```
cd $HOME/CFDEM
mv CFDEMcoupling-PUBLIC CFDEMcoupling-PUBLIC-$WM_PROJECT_VERSION
```

Secondly, open the .bashrc document to set the environment by:

```
gedit ~/.bashrc
$HOME/CFDEM/CFDEMcoupling-PUBLIC-$WM_PROJECT_VERSION/src/
lagrangian/cfdemParticle/etc/bashrc
```

Adding the content in the block below at the end of the bashrc document to set the paths:

```
#=============================================#
#- source cfdem env vars
export CFDEM_VERSION=PUBLIC
export CFDEM_PROJECT_DIR=$HOME/CFDEM/
CFDEMcoupling-$CFDEM_VERSION-$WM_PROJECT_VERSION
export CFDEM_PROJECT_USER_DIR=$HOME/CFDEM/
$LOGNAME-$CFDEM_VERSION-$WM_PROJECT_VERSION
export CFDEM_bashrc=$CFDEM_PROJECT_DIR/src/lagrangian/
cfdemParticle/etc/bashrc
export CFDEM_LIGGGHTS_SRC_DIR=$HOME/LIGGGHTS/LIGGGHTS-PUBLIC/src
export CFDEM_LIGGGHTS_MAKEFILE_NAME=auto
export CFDEM_LPP_DIR=$HOME/LIGGGHTS/lpp/src
. $CFDEM_bashrc
#=============================================#
```

After setting up the environment, running the code below could check the previous steps:

```
source ~/.bashrc
cfdemSysTest
```

A.1.4 Installation of Third Party Software

OpenFOAM relies some third-party software packages, which includes Scotch/PT-Scotch, ParaView, CGAL Computational Geometry Algorithms Library(not essential). Scopch/PT-Scotch can be by going into the ThirdParty directory and run the Allwmake script:

```
./ALlwmake
```

ParaView could be compiled by running the makeParaView script:

```
./makeParaView
```

After a long time of compiling, the environment needs to be updated by typing

```
wmRefresh
```

A.1.5 Compilation of LIGGGHTS and CFDEMcoupling

The CFDEM project could be compiled by running:

```
cfdemCompCFDEMall
```

The LIGGGHTS could be compiled by running:

```
cfdemCompLIG
```

Appendix B

Software tutorial

B.1 LIGGGHTS Tutorial

An useful tutorial of LIGGGHTS could be found on the official website of CFDEM:https://www.cfdem.com/system/files/LIGGGHTS_Tutorial.pdf The basic consistent of a general case is:

Initialization, including the decision of units, $atom_style$, boundary(periodic or not) and domain declaration.

Set up, including material properties, particle insertion(particle region, particle properties, particle composition, the description of particle insertion-insertion rate, initial velocity,region), importation of mesh from cad, using the imported mesh as wall(then creating the type of wall?), defining the physics.

Detailed settings, including setting integrator, gravity vector, time step, thermodynamic output quantities, shaft rotations(if the case exists rotations), and then check over 1 time step by running the time step. The last is to create the imaging information for results?

Execution and further settings, while running is the main task in this part.

In more complicated cases, such as example 4 in the tutorial document, interforce such as drag force is introduced, which could be simulated by firstly using CFD to determine the flow field in the absence of solid phase and then applying the flow field to the DEM simulations.

The information of applied flow field is added in the section of setting up, by the method of adding region and addforce informations.

There are also some useful practices in the end of the tutorial document.

B.1.1 Commands

$atom_style\ style\ args$: The command define the style of atoms to be used in a simulation, which include styles of bond, charge, ellipsoid, full, line, molecular, tri, hybrid, sphere, granular, bond/gran, superquadric, convexhull, sph. The choice decides quantities are stored in each atom. For granular, it is a case of diameter equals 0.0 in sphere style. For more information, see the website:https://www.cfdem.com/media/DEM/docu/atom_style.html

$atom_modify\ keyword\ values$: The command modify properties of the atom style, while keyword includes map, first and sort. For which map value is array or hash, of which hash is slower and save more memory storage. THe keyword sort refers to a spatial soring or reordering of atoms within Nfreq timesteps, which returns atoms in the same bin adjacent to each other after reordering, which improve cache performance when pairwise interactions and neighbor lists are computed. For more information, see the website:https://www.cfdem.com/media/DEM/docu/atom_modify.html

boundaryxyz: The command set the style of boundaries for the global simulation box in each dimension, while x,y,z could have value of p-periodic, f-fixed, s-shrink-wrapped(The position of the face is set to encompass the atoms in the dimension), m-shrink wrapped with a minimum value. Noted that f,s,m are all non-periodic. For more information, see the website:https://www.cfdem.com/media/DEM/docu/boundary.html

*newtonflag*1*flag*2: The command turns Newton's third law on or off for pairwise and bonded interactions, with flag on or off for both pairwise and bonded interactions, flag 1 on or off for pairwise interactions, flag2 on or off for bonded interactions. Setting on means a modest savings in computation at the cost of two times more communication, setting the pairwise newton to off means that if two interacting atoms are on different processors, both processors compute their interaction and the resulting force information is not communicated-the interaction is computed by each processor more generally speaking. For more information, see the website:https://www.cfdem.com/media/DEM/docu/newton.html

communicatestylekeywordvalue: The command sets the style of inter-processor communication that occurs each timestep as atom coordinates and other properties are exchanged between neighboring processors and stored as properties of ghost atoms. The first part style is single or multi, of which single means each processor acquires information for ghost atoms that are within a single distance from its subdomain while the distance is the maximum of the neighbor cutoff for all atom type pairs. For systems with widely varying cutoffs for different type pairs, the multi style is faster, while each atom type is assigned its own distance cutoff for communication purposes and fewer atoms will be communicated-granular systems is automatically performed with single style. For the second part keyword is cutoff, group or vel. Cutoff allows to set a ghost cutoff distance, with cutoff value Rcut(distance units); group limits communication to atoms in the specified group and all atoms will still migrate to new processors as they move, with group value group-ID; Vel enables velocity information to be communicated with ghost particles, with vel values yes or no, while yes means that ghost atoms store these quantities and no means not. To set as yes is needed by some pair styles which require the velocity state of both I and J particles to compute a pairwise I,J interaction. For more information, see the website:https://www.cfdem.com/media/DEM/docu/communicate.html

regionIDstyleargskeywordarg: The command defines a geometric region of space. The style part defines the type of region, which includes delete(no args), block, cone, cylinder, plane, prism, sphere, mesh/tet, union, intersect, wedge. The keyword part, includes side(value in or out, determines whether the region is considered to be inside or out side), units(lattice or box. determines the meaning of the distance units used to define the region), move(value v_x or v_y or v_z), rotate(value $v_theta, pxpypz, rxryrz$) determines the type or points position. For more information, see the website:https://www.cfdem.com/media/DEM/docu/region.html

processorsPxPyPzkeywordargs: The command specify how processors are mapped as a 3d logical grid to the global simulation box, while px, py, pz represents the processors in each dimension of 3d grid overlaying the simulation domain, which means the decomposition of the domain. For more information, see the website:https://www.cfdem.com/media/DEM/docu/processors.html

$create_boxNregion - ID$: The domain creates a simulation based on a specified region. For more information, see the website:https://www.cfdem.com/media/DEM/docu/create_box.html

neighbor: The command set parameters that affect the building of pairwise neighbor lists. Another command $neigh_modify$ command is set to yes if the skin distance is used to determine how often atoms migrate to new processors, while atoms are

migrated to new processors on the same timestep that neighbor lists are re-built. The type of what algorithm is used to build the list is determined by the part style, which includes 3 values: bin, nsq and multi, of which the bin style creates the list by binning which is an operation that scales linearly with N/P, the number of atoms per processors where N equals total number of atoms and P represents the number of processors with the bin size set to 0.5 of the largest cutoff distance between any pair of atom types. The multi style is a modified binning algorithm which is useful for systems with a wide range of cutoff distances, such as due to different size particles with the bin size set to 0.5 of the shortest cutoff distance. For more information, see the website:https://www.cfdem.com/media/DEM/docu/neighbor.html

$neigh_modify$: The command set parameters that affect the building and use of pairwise neighbor lists. The every, delay check, once options affect how often lists are built as a simulation runs. he delay setting means never build a new list until at least N steps after the previous build. The every setting means build the list every M steps (after the delay has passed). If the check setting is no, the list is built on the 1st step that satisfies the delay and every settings. If the check setting is yes, then the list is only built on a particular step if some atom has moved more than half the skin distance (specified in the neighbor command) since the last build. If the once setting is yes, then the neighbor list is only built once at the beginning of each run, and never rebuilt, which should only be done when atoms do not move far enough that the list should be rebuilt. For more information, see the website:https://www.cfdem.com/media/DEM/docu/neigh_modify.html

$fixIDgroup-IDstyleargs$: The command set a fix that will be applied to a group of atoms, while a fix is any operation that is applied to the system during timestepping or minimization, including updating of atom positions and velocities due to time integration, controlling temperature, applying constraint forces to atoms, enforcing boundary conditions, computing diagnostics, etc. For more information, see the website:https://www.cfdem.com/media/DEM/docu/fix.html

$pair_stylestyleargs$: The command determines the types of pair styles, for which pair potentials are defined between pairs of atoms that are within a cutoff distance and the set of active interactions typically changes over time. Hybrid models where specified pairs of atom types interact via different pair potentials can be setup using the hybrid pair style. The coefficients associated with a pair style are typically set for each pair of atom types, and are specified by the $pair_coeff$ command. The command $pair_modify$ sets options for mixing of type I-J interaction coefficients. For more information, see the website:https://www.cfdem.com/media/DEM/docu/pair_coeff.html and https://www.cfdem.com/media/DEM/docu/pair_coeff.html

$groupIDstyleargs$: The command identify a collection of atoms as belonging to a group, while the group ID could be used in other commands. If the group ID already exists, the group command adds the specified atoms to the group. The style part in the command includes delete or region or type or id or molecule or variable or subtract or union or intersect, with the delete style of the command also allows to remove the named group which is not used anymore; The region style puts all atoms in the region volume into the group, which is a static one-time assignment. The type, id and molecule styles put all atoms with the specified atom types, atom IDs or molecule IDs into the group, which can use arguments specified in one of two formats. For more information, see the website:https://www.cfdem.com/media/DEM/docu/group.html.

$compute$: The command defines a computation that will be performed on a group of atoms, which performs in a format of $computeIDgroup-IDstylegeneral_keywordsgeneral_valuesargs$. The style includes a list of possible style names, which will be discussed in the later

section. For more information, see the website:https://www.cfdem.com/media/DEM/docu/compute.html.

dumpIDgroup − IDstyleNfileargs: The command dumps a snapshot of atom quantities to one or more files every N timesteps in one of several styles, of which the image style is the exception. Only information for atoms in the specified group is dumped. For more information, see the website:https://www.cfdem.com/media/DEM/docu/dump.html.

B.1.2 fix styles

B.2 OpenFOAM tutorial

A fully explained tutorial could be found on the official website of OpenFOAM:https://www.openfoam.com/documentation/user-guide/index.php

The basic structure for a OpenFOAM case usually contains a constant directory(which contains a full description of the case mesh in a subdirectory and files specifying physical properties for the concerned application), a system directory(which is used for setting parameters associated with the solution procedure, including controlDict, fvSchemes, fvSolution, blockMeshDict) and the time directories(which contains individual files of data for particular fields).

B.2.1 tips of basic file format

1. dimensional units

Country List			
No.	Property	SI unit	USCS unit
1	Mass	kilogram(kg)	pound-mass(lbm)
2	Length	meter(m)	foot(ft)
3	Time	second(s)	second(s)
4	Temperature	Kelven(K)	degree Rankine(R)
5	Quantity	kilogram-mole(kgmol)	pound-mole(lbmol)
6	Current	ampere(A)	ampere(A)
7	Luminous intensity	candela(cd)	candela(cd)

For example, nu=[0 2 -1 0 0 0 0] means the unit of nu is $m^2 \cdot s_{-1}$.

2. Mesh generation with *blockMesh* utility The blocks of meshes are defined as: vertex numbering, number of cells and cell expansion ratios.The third part gives the cell expansion ratios for each direction in the block, which enables the mesh to be graded or refined in specified directions, including simplegrading and edgegrading.

3. time step choosing To determine timestep, Courant number is introduced: $C_o = \frac{\partial |t|}{\partial x}$, which needs to be smaller than 1, to achieve temporal accuracy and numerical stability. For meshes with different shapes, the smallest cell, ∂x_s is given by: $\partial x_s = l\frac{r-1}{\alpha r-1}$, while the ratio is given by: $r = R^{\frac{1}{n-1}}$, and α is given by: $\alpha = R$ when R>1, $\alpha = 1 - r^{-n} + r^{-1}$ when R<1.

"modelType" refers to the formulation of the equations to be solved. Choose "A", "B" or "Bfull", according to Zhou et al. (2010): "Discrete particle simulation of particle-fluid flow: model formulations and their applicability", JFM. "A" requires the use of the force models gradPForce and viscForce, whereas "B" requires the force

model “Archimedes”. “Bfull” refers to model type I, “A” refers to model type II and “B” refers to type III in the nomenclature used by Zhou et al.

B.3 CFDEM tutorial

In a CFDEM case, the codes are divided into two parts: CFD and DEM, while CFD folder includes the settings of fluid phase and the coupling settings, while DEM folder includes the settings of solid phase.

In DEM folder, the initial settings of particles is set in the file $in.liggghts_init$, with the region, properties, atom types defined. In CFD folder, .../0 folder stores the initial values of parameters, such as velocity, temperature, pressure, k-epsilon model parameters, while the boundary condition is also set by editing these files. the transport and turbulence properties is set by editing the files in .../constant folder, which defines the turbulence model and some parameters of the flow, such as prandtl number and viscosity. The file liggghtsCommands includes two parts, including a list of "liggghtsCommandModels", and then the settings for each model, which includes the starting up of reading the LIGGGHTS-input-script and other user-defined commands. The file couplingProperties defines the setup of the coupling routines of the CFD-DEM simulation, including sub-model settings and sub-model properties, while in model setting part, different model types are defined and in model properties part, the parameters of different types are introduced.

For the case of a fluidized bed, the force model attracts more attention, while different force models are introduced in the tutorial documentation on the website mentioned before: In the description, one could easily found the source of these

forceModel_Archimedes	*forceModel_ArchimedesIB*
forceModel_DiFeliceDrag	*forceModel_GidaspowDrag*
forceModel_KochHillDrag	*forceModel_LaEuScalarTemp*
forceModel_MeiLift	*forceModel_SchillerNaumannDrag*
forceModel_ShirgaonkarIB	*forceModel_checkCouplingInterval*
forceModel_fieldStore	*forceModel_fieldTimeAverage*
forceModel_gradPForce	*forceModel_noDrag*
forceModel_particleCellVolume	*forceModel_particleVolume*
forceModel_scalarGeneralExchange	*forceModel_virtualMassForce*
forceModel_viscForce	*forceModel_volWeightedAverage*

models and mathematic model from essay mentioned.

B.4 liggghts

1.initialization: creating particles-set parameters, defining(style of atom, boundary type, units, atom-modify to define data structure, newton’s third low on or off, dimension if not 3 dimensions)

2. definition: defining particles, read from files or create atoms on a lattice. region, define the region, create-box, create the box,

3. settings:

papers: 1. Influence of rolling friction on single spout fluidized bed simulation

2. ErgunTetMPI

3. cylinder bed: onset velocity of circulating fluidization and particle residence time distribution: a cfd-dem study

Appendix C

Different van der waals model test

C.1 Model Settings

C.1.1 Modified Van der waals Force Model

All models mentioned before, hertz contact model is selected, which corresponds to a soft sphere model and overlap exists when particles suffer a collision. In this case, when smaller Young's modulus value is used in computing instead of the real value, the particles would overlap more and thus leads to part of more-done work. In order to preserve this work, a modified model of van der waals model is introduced by Y. Gu et al [30], which is shown in figure C.1 with its expression equations given by C.1.

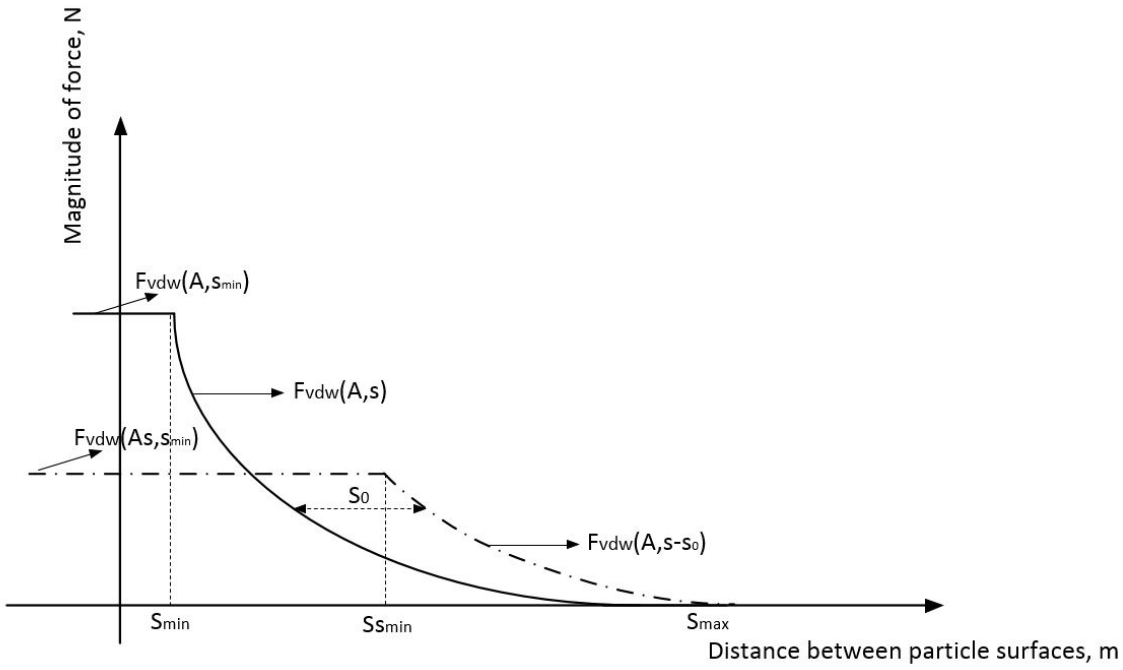

FIGURE C.1: Scheme of soft sphere model

$$\boldsymbol{f}_{v,ij} = \begin{cases} -F_{vdw}(A^R, s - s_0)\boldsymbol{n}_{ij} & s^S_{min} < s < s_{max} \\ -F_{vdw}(A^S, s^R_{min})\boldsymbol{n}_{ij} & s \leq s^S_{min} \end{cases} \tag{C.1}$$

While in the equation, A^S expresses the Hamaker constant for softer case and A^R represents the Hamaker constat for real case; s^S_{min} is the minimum separation distance for softer case and s^R_{min} the minimum separation distance for the real case;

s_0 is the distance between the original model and new model, where s_0 and s^S_{min} meet the equations:

$$F_{vdw}(A^S, s^R_{min}) = F_{vdw}(A^R, s^S_{min} - s_0) \tag{C.2}$$

$$F_{vdw}(A^R, s^R_{min}) \cdot s^R_{min} + \int_{S^R_{min}}^{s_{max}} F_{vdw}(A^R, s)ds = F_{vdw}(A^S, s^R_{min}) \cdot s^S_{min} + \int_{s^S_{min}}^{s_{max}} F_{vdw}(A^R, s - s_0)ds \tag{C.3}$$

From equations C.2 and C.3, for certain value of A_S,A_R, S^R_{min}, the value of s_0 and s^S_{min} could be calculated out through math tools. Thus a set of parameters of the case for modified van der waals force model are shown in table C.1.

TABLE C.1: Model parameters for the modified van der Waals force model

Case name	$Y_R(Pa)$	$Y_S(Pa)$	$s^R_{min}(m)$	$s^S_{min}(m)$	$s_0(m)$
4a	10^8	10^7	1×10^{-9}	3.434×10^{-9}	1.854×10^{-9}
4b	10^8	5×10^7	1×10^{-9}	1.490×10^{-9}	3.416×10^{-10}

C.1.2 Inter-coefficient Model

Except from using van der waals force model, sjkr cohesive model is also used widely, which only consider cohesive force when particles contact with each other. Suppose the contact area to be A, the additional normal force tends to maintain the contact, which writes:

$$F = kA \tag{C.4a}$$

$$A = \frac{\pi}{4}\frac{(d - r_i - r_j)(d + r_i - r_j)(d - r_i + r_j)(d + r_i + r_j)}{d^2} \tag{C.4b}$$

or

$$A = 2\pi\delta n 2R^* \tag{C.4c}$$

with k the cohesion energy density in J/m3 and d the distance between two particle centers.

The main difference between van der waals model and sjkr is that sjkr cohesive force only exists when particles contact with each other while in van der waals model, cohesive force exists even when particles do not contact, thus particles would suffer more. In this case, a comparison is also made with cohesionEnergyDensity set to be 15000 as an average value for cohesive particles.

The case of sjkr model corresponds to case 3 in the analysis below.

C.2 Results

C.2.1 Pressure Drop

Pressure drop plot for original case2(original vdW force model), case 3(orange line) and case4(4a cyan line, 4b magenta line) are shown in figure C.2, which shows the pressure drop change tendency of different kinds of cohesive models. It is shown that the stable value of pressure drop of case 2 is only 10Pa, about 5Pa lower than case 3 and 4, while the time when steady is reached is almost the same at 0.15s. For case 3, the line is quite similar to the line of case in in figure C.2, except the time. For

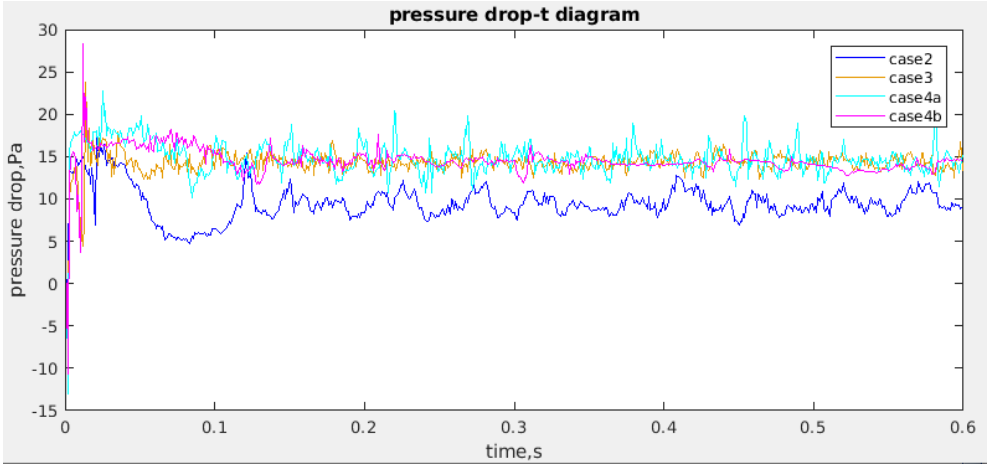

FIGURE C.2: Pressure drop diagram versus time of 2,3,4a,4b

the two lines of case 4, the fluctuation amplitude differs: the fluctuation of case 4a is larger than case 4b and much larger than case 3.

The phenomenon could also be explained by an assumption. For case 3, the cohesive force is only considered into account when particles contact with each other, which is like an additional force applied when compared to the case without cohesion, thus the properties of case 3 is the quite similar to the case of no-cohesion case. For case 4, the model of van der waals force is modified as figure C.1 shows, which is smaller than the original moedl, thus the motion of air molecules would suffer a smaller impact from cohesive force. For case 4a, the value of Youngs' modulus is smaller than case 4b, thus the modification of 4a model would be larger than 4b model, which corresponds the fact the fluctuation amplitude of case 4b quite the same with the line for the case of original case, but smaller than the value for case 4a.

C.2.2 Screen Snapshots

The snapshots of case 3, 4a and 4b are shown in figure C.3, while the screen of case 3 is a little similar to the non-cohesion case, the main difference between these two cases are the area of blue part, case 3 is more than the non-cohesion case, which also indicates that in case 3 cohesive force is considered but not large, thus the number of bubbles of case 3 is still large.

For case 4a and 4b shown in figure C.3, the motion of particles are quite similar to the original cohesion case 2. However, differences are also notable. For case 4b, there still exists slugging phenomenon, although much weaker than the one in case 2, while in case 4a, the slugging phenomenon almost disappears and the blue area also decreases. This could be explained by an assumption: when the surface difference between particles s is smaller than a certain value, the cohesive force of case 4a is smaller than case 4b, thus the particles would not contact so tight with each other in case 4a, which corresponds to the fact that the elimination of slugging phenomenon and smaller area of blue part.

C.2.3 Bubble Size

From figure C.4 it is shown that for different kinds of cohesive force models, the bubble probability distribution also differs. For case 3 with sjkr cohesion model, the

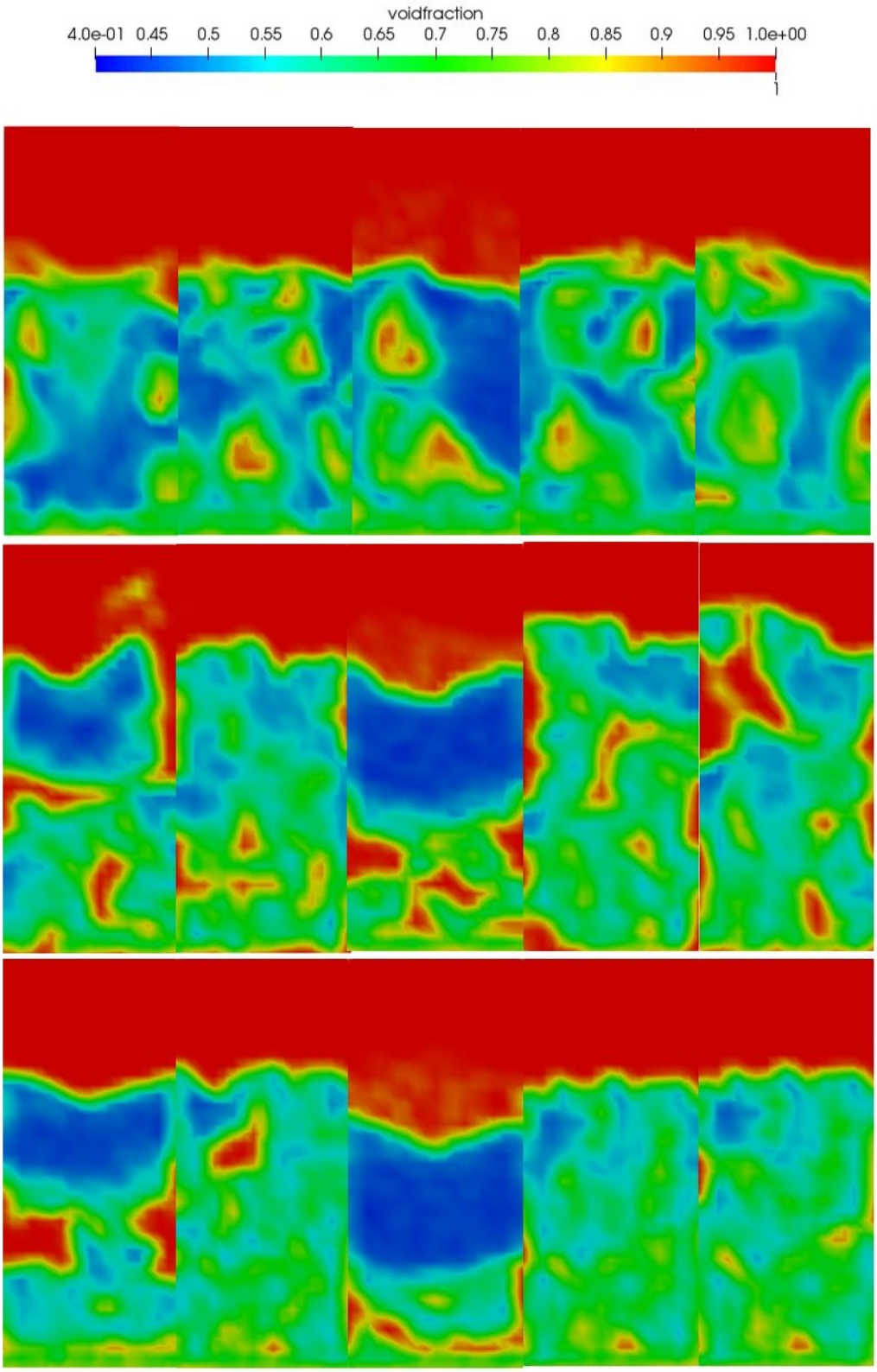

FIGURE C.3: Snapshots at different time points0.05s,0.1s,0.3s,0.33s,0.36s of case 3,4a,4b

probabilities of most kinds of bubbles are larger than case 2, which indicates that sjkr cohesion model only reflects parts of cohesive force;

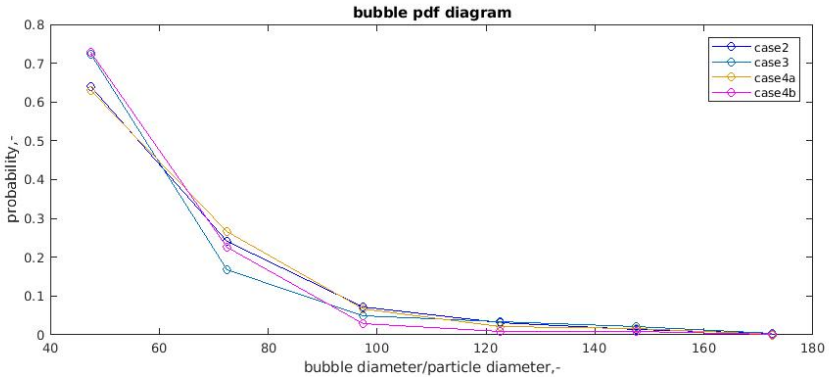

FIGURE C.4: Pdf plot of bubble diameters of case 2,3,4a,4b

C.2.4 Vector Plot

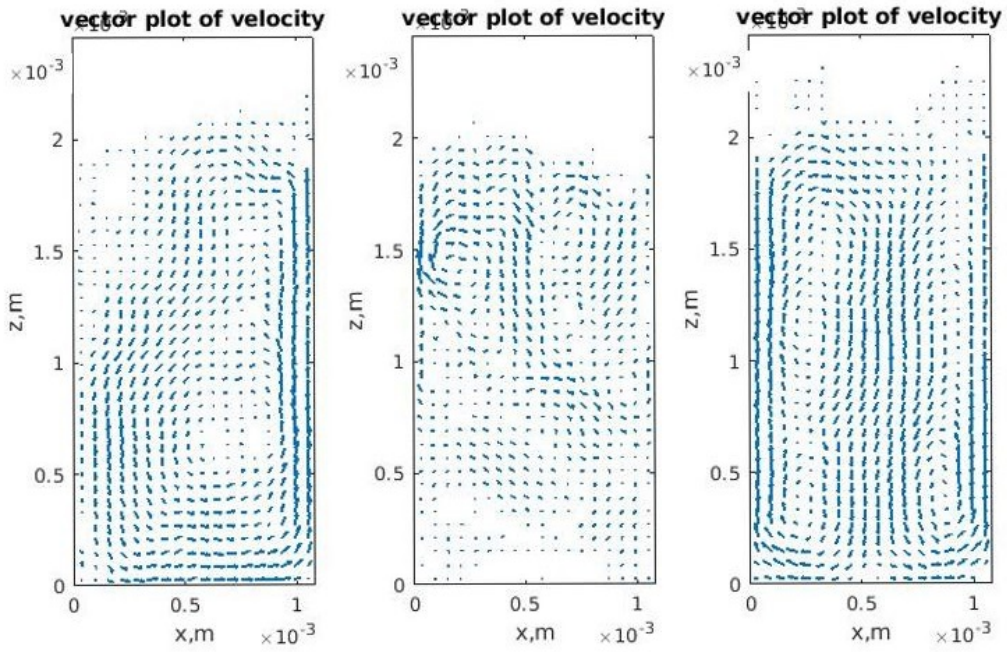

FIGURE C.5: Vector plot of case 4a,4b,3

In figure C.5, the first and second diagram shows the velocity vector of case 4a and 4b, the modified van der waals force model case. There exists only one circle in case 4a and 4b, which is similar to the result in the original vdW case in chapter 4.

the motion properties of particles are most similar to the original case, thus the shape of velocity vector plot, which is shown at the right side of figure C.5.

Appendix D

Hamaker Constant Analysis

As mentioned in section 5.1, the van der waals force is amplified in order to observe the effect of cohesive force on large particles, another important parameter is the Hamaker constant. With the increase of Hamaker constant, the strong pressure fluctuation is found due to the breakage of agglomerates [25]. Figure D.1 shows the pdf plot of agglomeration sizes with different Hamaker constant, from which it could be found that the larger the Hamaker constant, the larger the size of particle agglomerates. When Hamaker constant is decreased to 0, the case becomes a non-cohesion simulation.

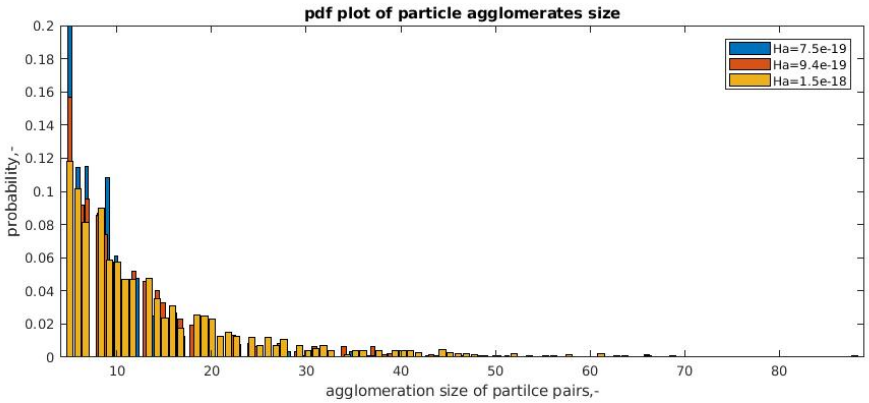

FIGURE D.1: Pdf plot of agglomeration size with different Hamaker constant number

Appendix E

Force Analysis

Figure E.1 and E.10 shows the average value of force magnitude on each particle at different time points of all cases(case 1 the non-cohesion case, case 2 the original vdW model case, case 3 the sjkr model case, case 4 the modified vdW case and case 5 the acoustic case). In figure E.1, it could be found that the average force magnitude over a certain period of case 1 and case 2 are almost equal to each other, with a value of 4e-10N, however, the fluctuation of the cohesion case is much larger, with the maximum fluctuation about 4e-10N. When acoustic force is added, the magnitude of total force decreases to a value of 3e-10N. As figure E.2 shows, sjkr force model is similar to the original non-conhesion model, while for modified van der waals force model 4a and 4b, the value of force magnitude is much smaller than the original van der waals model.

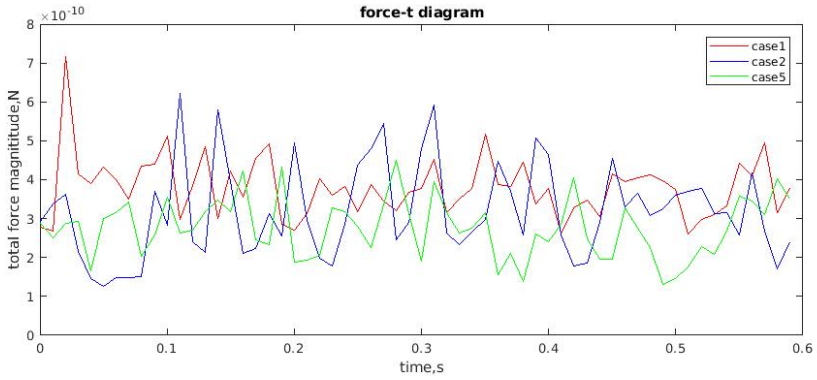

FIGURE E.1: Force diagram versus time of case 1,2,5

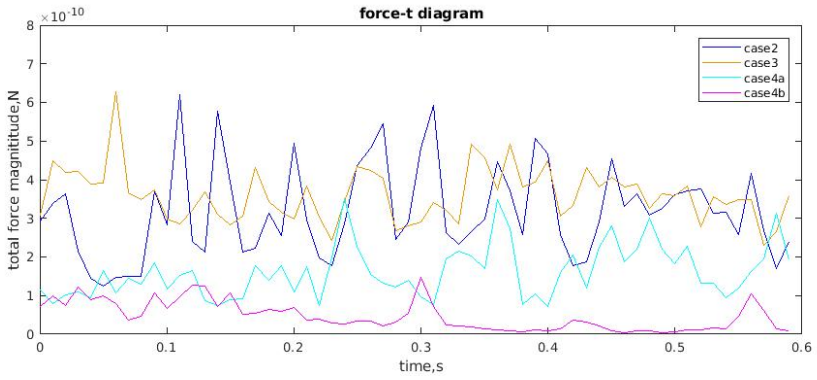

FIGURE E.2: Force diagram versus time of case 2,3,4a,4b

Appendix F

Matlab Codes

F.1 Detecting Bubbles

```
j=1;
k=1;
m=1;
ii=1;
jj=1;
bbn=1;
bbd=1;
Vo=cell(T,1);
Bo=cell(T,1);
w=0.054;
h=0.15;
for i=1:T
    m=1;
for j=1:nh
    k=nw*j;
    Vo{i}(j,:)=Data(m:k,i);
    j=j+1;
    m=(j-1)*nw+1;
end
end

for k=1:T
for i=1:nh
    for j=1:nw
        if Vo{k}(i,j)>=0.8
            Bo{k}(i,j)=1;
        else
            Bo{k}(i,j)=0;
        end
        j=j+1;
    end
    i=i+1;
end
Vg{k}=sum(Bo{k});
Vb(k)=sum(Vg{k});
end
```

```
for klm=1:T
[a,b]=find(Bo{klm}~=0);
c=[a,b];
aa=length(a);
gg=1;
M=zeros(aa,1);
bbnt=0;
bbdt=zeros(aa,3);
tt=1;
for jj=1:nw
     M=zeros(aa,1);
     gg=1;
      tt=1;
          for kk=1:aa
     if c(kk,2)==jj
         M(gg)=c(kk,1);
          gg=gg+1;
     end
     kk=kk+1;
          end
          N=find(M~=0);
          bb=length(N);
          Mn=M(1:bb+1);
  while tt<=bb
     if Mn(tt+1)==Mn(tt)+1
          bbnt=bbnt+1;
          bbdt(bbnt,2)=Mn(tt);
          bbdt(bbnt,1)=1;
          bbdt(bbnt,3)=jj;
          pp=tt;
            while Mn(pp+1)==Mn(pp)+1
            bbdt(bbnt,1)=1+bbdt(bbnt,1);
            pp=pp+1;
            end
          tt=pp+1;
     else
          bbnt=bbnt+1;
          bbdt(bbnt,1)=1;
          bbdt(bbnt,2)=Mn(tt);
          bbdt(bbnt,3)=jj;
          tt=tt+1;
     end
  end
end

Vbb=sum(bbdt(:,1));

iii=1;
jjj=1;
kkk=1;
row=nw;
col=nh;
```

```
E=cell(1,row);
for jjj=1:row
    iii=1;
    kkk=1;
    for iii=1:kk-1
        if bbdt(iii,3)==jjj
            E{jjj}(kkk,1)=bbdt(iii,1);
            E{jjj}(kkk,2)=bbdt(iii,2);
            E{jjj}(kkk,3)=bbdt(iii,3);
            kkk=kkk+1;
        end
        iii=iii+1;
    end
    jjj=jjj+1;
end

ir=1;
ic=1;
EE=E;
for ir=1:row-1
    if ~isempty(E{1,ir+1}) & ~isempty(E{1,ir})
    ica=length(E{1,ir}(:,1));
    icca=length(E{1,ir+1}(:,1));
    ic=1;
    icc=1;
    for ic=1:ica
        for icc=1:icca
                nhi=EE{1,ir+1}(icc,1);
                nlo=EE{1,ir}(ic,1);
                phi=E{1,ir+1}(icc,2);
                plo=E{1,ir}(ic,2);
                zz=1;
                   if phi==plo
                        EE{1,ir+1}(icc,1)=nhi+nlo;
                        EE{1,ir+1}(icc,2)=phi;
                        EE{1,ir}(ic,1)=0;
                   else if nhi~=1
                           for zz=1:nhi-1
                               if phi+zz==plo
                                   EE{1,ir+1}(icc,1)=nhi+nlo;
                                   EE{1,ir+1}(icc,2)=phi+zz;
                                   EE{1,ir}(ic,1)=0;
                               end
                           end
                       else if nlo~=1
                               for zz=1:nlo-1
                                   if plo+zz==phi
                                       EE{1,ir+1}(icc,1)=nhi+nlo;
                                       EE{1,ir+1}(icc,2)=phi;
                                       EE{1,ir}(ic,1)=0;
                                   end
                               end
```

```
                                end
                            end
                        end
                end
            end
            E{1,ir}=EE{1,ir};
            E{1,ir+1}=EE{1,ir+1};
            end
end


%Z{klm}=zeros(Vb(klm),3);
Z{klm}=cell2mat(E');
yy=1;
aay=length(Z{klm});
%ZZ=zeros(aay,4);
wg=w/row;
hg=h/col;

for qq=1:aay
        if Z{klm}(qq,1)~=0
         ZZ{klm}(yy,1)=Z{klm}(qq,1);
         ZZ{klm}(yy,2)=Z{klm}(qq,2);
         ZZ{klm}(yy,3)=Z{klm}(qq,3);
         ZZ{klm}(yy,4)=nthroot(ZZ{klm}(yy,1)*wg*hg*3/(4*pi),3);
         yy=yy+1;
        end
end

dbb{klm}=ZZ{klm}(:,4);
%V{klm}=sum(Z{klm}(:,1));
%DD=nthroot(V{klm}*wg*hg*3/(4*pi),3);
%lz=1;
%aaz=length(ZZ{klm})
%for lzz=1:aaz
 %    if ZZ{klm}(lzz,1)~=0
  %       lz=lz+1;
  %  end
%end
%db(:,klm)=ZZ{klm}(1:lz-1,4);
%dm(klm,1)=mean(db);
%dm(klm,2)=klm*0.0001;

end

%ldm=length(dm);
%j=1;
%DM=zeros(45,2);
%for i=1:ldm
 %if dm(i,1)~=0
  %   DM(j,1)=dm(i,1);
   %  DM(j,2)=dm(i,2);
```

```
    % j=j+1;
 %end
%end
%plot(DM(:,2),DM(:,1));

for klm=2:T
    A=max(dbb{klm});
    rowmax=find(dbb{klm}==A);
    dbb{klm}(rowmax)=[];
end

for klm=2:T
    if isempty(dbb{klm})
        dbb{klm}=0;
    end
end
DB1=cell2mat(dbb');

F0=find(DB1==0)
DB1(F0)=[];
d=1e-3;
DBB=DB1/d;
pdfplot(DBB,10);
title('pdf plot of bubble size')
xlabel('bubble diameter/particle diameter,-')
ylabel('probability,-')
```

F.2 Bed Height Plot

```
% find bed height%
j=1;
k=1;
m=1;
ii=1;
jj=1;
bbn=1;
bbd=1;
Vo=cell(T,1);
Bo=cell(T,1);
lf=zeros(T,nw);
w=0.00108;
h=0.00252;
for i=1:T
    m=1;
for j=1:nh
    k=nw*j;
    Vo{i}(j,:)=Data(m:k,i);
    j=j+1;
    m=(j-1)*nw+1;
end
end
```

```
for k=1:T
for i=1:nh-4
    for j=1:nw
        if Vo{k}(i,j)<0.8
            Bo{k}(i,j)=1;
        end
        j=j+1;
    end
    i=i+1;
end
Vg{k}=sum(Bo{k});
Vb(k)=sum(Vg{k});
end

for k=1:T
    for j=1:nw
            Fo=find(Bo{k}(:,j)==1);
            lf(k,j)=max(Fo);
    end
    lff(k)=mean(lf(k,:));
end


bh=lff*6e-5;
t=[0:599]*0.001;
plot(t,lff);
```

F.3 Find Agglomerations

```
r=1e-5;
N=km+1;
pair=cell(1,N);
for i=1:N
    pp=p{i};
    pp(:,4)=ones(Nc,1);
    z=1;
    for j=1:Nc
        t=j+1;
        k=t;
          for k=t:Nc
              n=pp(j,4)+pp(k,4);
              jx=pp(j,1);
              jy=pp(j,2);
              jz=pp(j,3);
              kx=pp(k,1);
              ky=pp(k,2);
              kz=pp(k,3);
              djk=sqrt((jx-kx)^2+(jy-ky)^2+(jz-kz)^2);
                  if djk<=r*2
               pair{i}(z,1)=j;
               pair{i}(z,2)=k;
               z=z+1;
```

```
                    end
                  k=k+1;
                end
    end
      sum(pp(:,4));
end



for ii=1:N
    lz=length(pair{ii});
    pp=1;
    pairnew=cell(Nc,1);
    %zz=1;
    for pp=1:Nc
        zz=1;
        for jj=1:lz
        %zz=1;
        if pair{ii}(jj,1)==pp
        pairnew{pp}(zz,1)=pair{ii}(jj,1);
        pairnew{pp}(zz,2)=pair{ii}(jj,2);
        zz=zz+1;
        end
        end
    end
    lzz=lz;
    tt=1;
    while tt<=length(pair{ii}(:,1))
        ttk=tt+1;
        kk=ttk;
        while kk<=length(pair{ii}(:,1))
        if pair{ii}(tt,2)==pair{ii}(kk,2)
              tt1=pair{ii}(tt,1);
              kk1=pair{ii}(kk,1);
              if ~isempty(pairnew{kk1})&~isempty(pairnew{tt1})
              la=length(pairnew{tt1}(:,1));
              lb=length(pairnew{kk1}(:,1));
              for gg=1:lb
                   pairnew{tt1}(la+gg,1)=kk1;
                   pairnew{tt1}(la+gg,2)=pairnew{kk1}(gg,2);
              end
              pairnew{kk1}=[];
              end
             %kk=ttk;
            %kk=kk+1;
        end
        %lzz=length(pair{ii});
        kk=kk+1;
        end
        tt=tt+1;
    end
```

```
        for jjj=1:Nc
            ttk=jjj+1;
            kkk=ttk;
            for kkk=ttk:Nc
                if ~isempty(pairnew{jjj})&~isempty(pairnew{kkk})
                    laa=length(pairnew{jjj}(:,1));
                    %lbb=length(pairnew{kkk}(:,1));
                    for jj1=1:laa
                        %for jj2=1:lbb
                            jj2=1;
                            while (~isempty(pairnew{kkk})&jj2<=length(pairne
                            if pairnew{jjj}(jj1,2)==pairnew{kkk}(jj2,2)
                                rowvalue=pairnew{kkk}(jj2,1);
                                rowname=find(pairnew{kkk}(:,1)==rowvalue);
                                lrow=length(rowname);
                                for gg=1:lrow
                                pairnew{jjj}(laa+gg,:)=pairnew{kkk}(rowname(
                                end
                                for ggg=1:lrow
                                pairnew{kkk}(rowname(1),:)=[];
                                ggg=ggg+1;
                                end
                                lbb=length(pairnew{kkk}(:,1));
                            end
                            jj2=jj2+1;
                            end
                        %end
                    end
                end
            end
        end
        pairr{ii}=pairnew;
end

for ii=1:N-1
    pair1=pairr{ii};
    pair2=pairr{ii+1};
    for j=1:Nc
        lp1=0;
        lp2=0;
        if ~isempty(pair1{j})&isempty(pair2{j})
            pair1{j}=[];
        else
            if ~isempty(pair1{j})&~isempty(pair2{j})
            lp1=length(pair1{j}(:,1));
            lp2=length(pair2{j}(:,1));
            if lp1==lp2
                difference=pair1{j}-pair2{j};
                d1=difference(:,1);
                d2=difference(:,2);
                k1=find(d1~=0)
                k2=find(d2~=0)
```

```
                if ~isempty(k1)|~isempty(k2)
                    if ~isempty(k1)
                        k11=length(k1);
                        if ~isempty(k2)
                            k22=length(k2);
                        else
                            k22=0;
                        end
                    else
                        k11=0;
                        k22=length(k2);
                    end
                 k0=max(k11,k22);
                 kk=1;
                while(kk<=lp1&~isempty(pair1{j})&k0>0)
                    if difference(kk,2)~=0|difference(kk,1)~=0
                        pair1{j}(kk,:)=[];
                        kk=kk-1;
                        k0=k0-1;
                    end
                    kk=kk+1;

               end
                end
            else if lp1>lp2
                    kk=1;
                    lajkfd=lp1;
                     while(kk<=lp2&~isempty(pair1{j})&kk<=lajkfd)
                        if pair1{j}(kk,1)~=pair2{j}(kk,1)|pair1{j}(kk,2)~=pair
                            pair1{j}(kk,:)=[];
                            kk=kk-1;
                            lajkfd=lajkfd-1;
                        end
                        kk=kk+1;
                     end

                if ~isempty(pair1{j})
                lpp1=length(pair1{j}(:,1));
                lpp2=length(pair2{j}(:,1));
                if lpp1~=lpp2
                    pair1{j}(lpp1,:)=[];
                end
                end
                end
            end
            end
        end
    end
    pairs{ii}=pair1;
end
```

```
 for JJ=1:Nc
     AA=zeros(Nc,1);
     if ~isempty(pairs{ii}{JJ})
         lj=length(pairs{ii}{JJ}(:,1));
        AA=unique(pairs{ii}{JJ}(:,1));
         lj1=length(AA);
         sjz(JJ)=lj+lj1;
     end
 end

row0=find(sjz==0);
sjz(row0)=[];



%DB=cell2mat(placeb');
pdfplot(sjz,100);
title('pdf plot of agglomeration size')
xlabel('agglomeration size,m')
ylabel('probability,-')
```

F.4 Vector Plot of Velocity

```
nw=18;
nb=1;
nh=42;
w=0.00108;
b=0.00006;
h=0.00252;
N=km;
Np=10000;

dx=w/nw;
dy=b/nb;
dh=h/nh;

for ii=1:N
px(:,ii)=p{ii}(:,1);
py(:,ii)=p{ii}(:,2);
pz(:,ii)=p{ii}(:,3);

ux(:,ii)=u{ii}(:,1);
uy(:,ii)=u{ii}(:,2);
uz(:,ii)=u{ii}(:,3);

pp=1;
tt=1;
 for i=1:nh
    for k=1:nw
        pp=1;
        %uv=zeros(Np,N);
```

```
        for j=1:Np
          x=(k-1)*dx;
          x1=k*dx;
          h=(i-1)*dh;
          h1=i*dh;
          if x<px(j,ii)&px(j,ii)<x1&h<pz(j,ii)&pz(j,ii)<h1
              uv{ii}(pp,tt)=ux(j,ii);
              uu{ii}(pp,tt)=uz(j,ii);
              pp=pp+1;
          end
        end
        if pp~=1
          UU{ii}(tt,1)=mean(uv{ii}(:,tt));
          UU{ii}(tt,2)=mean(uu{ii}(:,tt));
          UU{ii}(tt,3)=k*dx-dx/2;
          UU{ii}(tt,4)=i*dh-dh/2;
          tt=tt+1;
        else
          UU{ii}(tt,1)=0;
          UU{ii}(tt,2)=0;
          UU{ii}(tt,3)=k*dx-dx/2;
          UU{ii}(tt,4)=i*dh-dh/2;
          tt=tt+1;
        end
    end
 end
end

UUU=zeros(tt-1,4);

gg=1;
for i=1:tt-1
for jj=1:N
    UUU(i,1)=UU{jj}(i,1)+UUU(i,1);
    UUU(i,2)=UU{jj}(i,2)+UUU(i,2);
end
end
UUU=UUU./N;
X=UU{1}(:,3);
Y=UU{1}(:,4);
Ux=UUU(:,1)
Uy=UUU(:,2);


q=quiver(X,Y,Ux,Uy);
title('vector plot of velocity')
xlabel('x,m')
ylabel('z,m')
axis equal
axis([0 w 0 h])
%q = quiver(1:10,1:10);
c = q.LineWidth;
```

```
q.LineWidth = 3.0;
```

Bibliography

[1] C. Dechsiri, *Particle transport in fluidized beds: experiments and stochastic models*. PhD thesis, University of Groningen, s.n., 2004.

[2] D. Geldart, "Types of gas fluidization," *Powder Technology*, vol. 7, no. 5, pp. 285 – 292, 1973.

[3] Q. Guo, X. Yang, W. Shen, and H. Liu, "Agglomerate size in an acoustic fluidized bed with sound assistance," *Chemical Engineering and Processing: Process Intensification*, vol. 46, no. 4, pp. 307 – 313, 2007.

[4] Y. Tatemoto, Y. Mawatari, T. Yasukawa, and K. Noda, "Effect of vibration on particle motion in two dimensional fluidized bed," *Chemical Engineering Science*, vol. 27, no. 6, pp. 824–826, 2001.

[5] Y. Tatemoto, Y. Mawatari, T. Yasukawa, and K. Noda, "Numerical simulation of particle motion in vibrated fluidized bed," *Chemical Engineering Science*, vol. 59, no. 2, pp. 437 – 447, 2004.

[6] Y. Tatemoto, Y. Mawatari, and K. Noda, "Numerical simulation of cohesive particle motion in vibrated fluidized bed," *Chemical Engineering Science*, vol. 60, no. 18, pp. 5010 – 5021, 2005.

[7] Q. Yu, R. N. Dave, C. Zhu, J. A. Quevedo, and R. Pfeffer, "Enhanced fluidization of nanoparticles in an oscillating magnetic field," *AIChE Journal*, vol. 51, no. 7, pp. 1971–1979.

[8] F. K. van Willigen, B. Demirbas, N. Deen, J. Kuipers, and J. van Ommen, "Discrete particle simulations of an electric-field enhanced fluidized bed," *Powder Technology*, vol. 183, no. 2, pp. 196 – 206, 2008.

[9] E. K. Levy, I. Shnitzer, T. Masaki, and J. Salmento, "Effect of an acoustic field on bubbling in a gas fluidized bed," *Powder Technology*, vol. 90, no. 1, pp. 53 – 57, 1997.

[10] R. D. Morse, "Sonic energy in granular solid fluidization," *Industrial Engineering Chemistry*, vol. 47, no. 6, pp. 1170–1175, 1955.

[11] P. Russo, R. Chirone, L. Massimilla, and S. Russo, "The influence of the frequency of acoustic waves on sound-assisted fluidization of beds of fine particles," *Powder Technology*, vol. 82, no. 3, pp. 219 – 230, 1995.

[12] R. Chirone, L. Massimilla, and S. Russo, "Bubble-free fluidization of a cohesive powder in an acoustic field," *Chemical Engineering Science*, vol. 48, no. 1, pp. 41 – 52, 1993.

[13] "Bubbling fluidization of a cohesive powder in an acoustic field," *Fluidization VII*, pp. 545–553.

[14] C. Herrera and E. Levy, "Bubbling characteristics of sound-assisted fluidized beds," *Powder Technology*, vol. 119, no. 2, pp. 229 – 240, 2001.

[15] C. A. Herrera, E. K. Levy, and J. Ochs, "Characteristics of acoustic standing waves in fluidized beds," *AIChE Journal*, vol. 48, no. 3, pp. 503–513.

[16] "Agglomerate particluate fluidization and e-particles," *Proceedings of the Third Joint China/USA Chemical Engineering Conference*, vol. Beijing, pp. 12–006.

[17] C. Zhu, G. Liu, Q. Yu, R. Pfeffer, R. N. Dave, and C. H. Nam, "Sound assisted fluidization of nanoparticle agglomerates," *Powder Technology*, vol. 141, no. 1, pp. 119 – 123, 2004.

[18] Q. Guo, Y. Li, M. Wang, W. Shen, and C. Yang, "Fluidization characteristics of sio2 nanoparticles in an acoustic fluidized," *Chemical Engineering & Technology*, vol. 29, no. 1, pp. 78–86.

[19] X. Ku, T. Li, and T. Løvås, "Influence of drag force correlations on periodic fluidization behavior in eulerian–lagrangian simulation of a bubbling fluidized bed," *Chemical Engineering Science*, vol. 95, pp. 94 – 106, 2013.

[20] Q. Guo, H. Liu, W. Shen, X. Yan, and R. Jia, "Influence of sound wave characteristics on fluidization behaviors of ultrafine particles," *Chemical Engineering Journal*, vol. 119, no. 1, pp. 1 – 9, 2006.

[21] Q. Guo, J. Zhang, and J. Hao, "Flow characteristics in an acoustic bubbling fluidized bed at high temperature," *Chemical Engineering and Processing: Process Intensification*, vol. 50, no. 3, pp. 331 – 337, 2011.

[22] C. Si, J. Zhou, and Q. Guo, "Characterization of pressure fluctuation signals in an acoustic bubbling fluidized bed," *Journal of the Taiwan Institute of Chemical Engineers*, vol. 42, no. 6, pp. 929 – 936, 2011.

[23] C. Si and Q. Guo, "Fluidization characteristics of binary mixtures of biomass and quartz sand in an acoustic fluidized bed," *Industrial & Engineering Chemistry Research*, vol. 47, no. 23, pp. 9773–9782, 2008.

[24] P. Ammendola, R. Chirone, and F. Raganati, "Fluidization of binary mixtures of nanoparticles under the effect of acoustic fields," *Advanced Powder Technology*, vol. 22, no. 2, pp. 174 – 183, 2011. Special issue of the 6th World Congress on Particle Technology.

[25] W. Shuai, L. Xiang, L. Huilin, L. Guodong, W. Jiaxing, and X. Pengfei, "Simulation of cohesive particle motion in a sound-assisted fluidized bed," *Powder Technology*, vol. 207, no. 1, pp. 65 – 77, 2011.

[26] U. Wankhede, R. Sonolikar, and S. Thombre, "Effect of acoustic field on heat transfer in a sound assisted fluidized bed of fine powders," *International Journal of Multiphase Flow*, vol. 37, no. 9, pp. 1227 – 1234, 2011.

[27] M. van der Hoef, M. van Sint Annaland, N. Deen, and J. Kuipers, "Numerical simulation of dense gas-solid fluidized beds: A multiscale modeling strategy," *Annual Review of Fluid Mechanics*, vol. 40, no. 1, pp. 47–70, 2008.

[28] X.-L. Zhao, S.-Q. Li, G.-Q. Liu, Q. Yao, and J.-S. Marshall, "Dem simulation of the particle dynamics in two-dimensional spouted beds," *Powder Technology*, vol. 184, no. 2, pp. 205 – 213, 2008. DISCRETE ELEMENT MODELLING OF FLUIDISED BEDS (Special Issue: Dedicated to Professor Yutaka Tsuji).

[29] Z. Y. ZHOU, S. B. KUANG, K. W. CHU, and A. B. YU, "Discrete particle simulation of particle–fluid flow: model formulations and their applicability," *Journal of Fluid Mechanics*, vol. 661, p. 482–510, 2010.

[30] Y. Gu, A. Ozel, and S. Sundaresan, "A modified cohesion model for cfd–dem simulations of fluidization," *Powder Technology*, vol. 296, pp. 17 – 28, 2016. Frontiers in Particuology - in Memory of Professor Mooson Kwauk.

[31] K. Chu, B. Wang, A. Yu, and A. Vince, "Cfd-dem modelling of multiphase flow in dense medium cyclones," *Powder Technology*, vol. 193, no. 3, pp. 235 – 247, 2009. Special Issue: Discrete Element Methods: The 4th International conference on Discrete Element Methods.

[32] M. S. van Buijtenen, W.-J. van Dijk, N. G. Deen, J. Kuipers, T. Leadbeater, and D. Parker, "Numerical and experimental study on multiple-spout fluidized beds," *Chemical Engineering Science*, vol. 66, no. 11, pp. 2368 – 2376, 2011.

[33] P. Morse and K. Ingard, *Theoretical Acoustics*. International series in pure and applied physics, Princeton University Press, 1986.

[34] K. Chu, B. Wang, D. Xu, Y. Chen, and A. Yu, "Cfd–dem simulation of the gas–solid flow in a cyclone separator," *Chemical Engineering Science*, vol. 66, no. 5, pp. 834 – 847, 2011.

[35] M. Urciuolo, P. Salatino, A. Cammarota, and R. Chirone, "Development of a sound-assisted fluidized bed filter/afterburner for particle-laden gas clean-up," *Powder Technology*, vol. 180, no. 1, pp. 102 – 108, 2008. Gas Cleaning at High Temperature: papers presented at the 6th International Symposium on Gas Cleaning at High Temperature, Osaka, Japan 20-22 October 2005.

[36] X. Wang, F. Rahman, and M. Rhodes, "Nanoparticle fluidization and geldart's classification," *Chemical Engineering Science*, vol. 62, no. 13, pp. 3455 – 3461, 2007. Frontier of Chemical Engineering - Multi-scale Bridge between Reductionism and Holism.